Aus dem Fachbereich Medizin der Philipps-Universität Marburg

Klinik für Neurologie Direktor Prof. Dr. med. Lars Timmerman

Titel der Dissertation:

Establishment of new experimental models of progressive prodromal Parkinson's disease using viral-mediated overexpression of wild-type human α-synuclein in the substantia nigra compacta and the locus coeruleus in mice

Inaugural-Dissertation zur Erlangung des Doktorgrades der gesamten Humanbiologie

dem Fachbereich Medizin der Philipps-Universität Marburg

vorgelegt von

Bolam Lee

aus Seoul, Südkorea

Marburg, 2019

Angenommen vom Fachbereich Medizin der Philipps-Universität Marburg am:
8. Februar 2019

Gedruckt mit Genehmigung des Fachbereichs.

Dekan: Prof. Helmut Schäfer
Referent: Prof. Dr. Wolfgang Oertel
1. Korreferent: Prof. Dr. Marco Rust

Thank God for every single step I have taken and thank my family for all the support

To design better therapeutics against Parkinson's disease (PD), it is of utmost importance to understand the pattern of α-synucleinopathy in key brain regions, which are considered to be crucial in the prodromal and manifest PD.

To answer this question, this dissertation consists of two different research efforts with a different focus as the following:

In Part I, a potential therapeutic candidate was employed in two classical in-vitro and in-vivo nigral dopaminergic model of PD to understand the relationship between the cholinergic anti-inflammatory pathway and α-synuclein.

In Part II, a newly established prodromal PD mouse model focused on the locus coeruleus and the vagal nuclear complex was characterized using multiple recombinant adeno-associated viral vectors (rAAV) carrying α-synuclein to investigate selective neuronal vulnerability and the synaptic transport.

All in all, this set of findings demonstrate novel insights from three different brain regions using α-synuclein in the PD research field for the first time. This collective report offers a new experimental mouse model of prodromal PD and thus may contribute to the disease-modifying compound development for PD in the future.

Index

I. Part 1.

JN403, α-7-nicotine-acetylcholine-receptor agonist, reduces alpha-synuclein induced inflammatory parameters in in-vitro microglia but fails to attenuate the reduction of TH immunoreactive nigral neurons in a focal alpha-synuclein overexpression mouse model of Parkinson's disease.

INTRODUCTION

Epidemiological studies show that smoking is associated with a reduced risk of Parkinson's disease (PD) along with other lifestyle factors, such as caffeine, physical activity and taking ibuprofen [1]. Regarding caffeine, a recent randomized controlled trial showed that twice daily consumption of caffeine-containing capsules for 18 months failed to show any (symptomatic or disease-modifying) beneficial effect as it did not improve PD motor symptoms in Parkinson patients with 1-8 years disease duration [27]. On the other hand, nicotine, a potent nicotinic acetylcholine receptor (nAChR) agonist, has also been considered as a therapeutic target as it exerted antidyskinetic activity in non-human primate models of dopamine-induced dyskinesias [6, 42]. However, so far clinical studies probing therapeutic efficacy in PD patients failed to show convincing effects e.g. on the improvement of motor symptoms [7, 38, 40]. Nevertheless, the 'cholinergic anti-inflammatory pathway' suggests that treatment with nicotinic agonists may modulate the production of proinflammatory cytokines from immune cells via activation of α-7-nicotine-acetylcholine-receptors (α7-nAChRs) as they are pivotal to inhibit synthesis and release of proinflammatory cytokines [17, 36, 39].

Several lines of evidence show that microglia-induced inflammation may not only be a consequence of neurodegeneration but also a trigger to dopaminergic cell loss during the course of the disease [15]. Chronically activated microglia release abundant proinflammatory mediators, such as nitric oxide (NO), tumor necrosis factor-α (TNF-α), and reactive oxygen species, which in turn may cause further microglia activation and neuronal loss. However, the precise role of microgliosis in PD still needs to be uncovered [12].

The hallmarks of PD are characterized by progressive depigmentation and subsequent loss of dopaminergic (DA) neurons in the substantia nigra pars compacta (SNc) [9] as well as the formation of eosinophilic cytoplasmic inclusions, referred to as Lewy bodies (LBs) in surviving nigral neurons. The major component of LBs is alpha-synuclein (αSyn), a protein of 140 amino acids that contains three functional domains: the N-terminal domain amino acid residues (AA 1-60), the NAC-region (AA 1-95) and the C-terminal domain (AA 96-140) [33]. Typically, αSyn lacks a definitive secondary structure, therefore, αSyn can obtain an α-helical or a β-sheet conformation [20, 37]. A

series of in-vitro and in-vivo studies revealed that αSyn released by damaged DA neurons accelerates reactive microgliosis and closely correlated with the progressive nature of neurodegeneration [15].

α7-nAChRs may serve as a crucial link between inflammation and neurodegeneration in PD and could represent a pharmacological target for potential neuroprotection [5, 34]. However, in-vivo research for understanding the potential efficacy of α7-nAChRs is restricted to a toxin (MPTP)-induced PD animal model [34]. Our previous research showed that MPTP-induced nigral dopaminergic cell loss was reduced, and the accompanying neuroinflammatory response was attenuated with a daily treatment of the α7-nAChR agonist, PNU-282987 [34]. These observations led to the question of whether the other α7-nAChR agonist, JN403 has the potential to modulate microglial function in-vitro and displays efficacy in-vivo in rodent models for PD. JN403 has been described as a potent and selective α7-nAChR agonist, shows good penetration into the brain after oral administration in rodents [10, 11] and is a potential candidate for clinical use.

The aim of this study is, therefore, to investigate the functional role of JN403 in microglia cell cultures treated with αSyn as well as in a focal in-vivo nigral αSyn overexpression mouse model of PD.

METHODS

Microglia cultures of the mouse ventral mesencephalon

The protocol of the microglia culture is identical as published before [29]. Briefly, microglia cultures derived from E13.5 mouse embryos (Janvier Breeding Center, France) were obtained by mild trypsinization as described previously. After 14 days, cultures were washed with Dulbecco's modified Eagle's medium/F-12 nutrient mixture (DMEM/F12; Invitrogen, Cergy-Pontoise, France) supplemented with 10% fetal calf serum (FCS) to eliminate the serum and then incubated with diluted DMEM/F12 (trypsin) 1:4 for 90 min at 37 °C until the astrocytic upper layer detached. The medium containing the layer of detached cells was aspirated, and the highly enriched microglial cell population that remained attached to the bottom of the well was exposed to 500 µL of DMEM/F12 with 10% FCS to allow trypsin inactivation. The remaining microglial cells were treated with JN403 (100 nM, 1 µM or 10 µM) for 24 hours followed by addition of human α-synuclein fragment (61-140) (rPeptide; Bogart, GA, USA) for another 24 hours.

MTT-assay

The cell viability was measured using the 3-(4,5-dimethylthiazol-2-yl)-2,5-diphenyltetrazolium bromide (MTT; Sigma-Aldrich, Steinheim, Germany) assay as described previously [23]. MTT was added to the cells at a final concentration of 0.5 mg/ml in the cell culture medium, and the cells were incubated for 30 min at 37 °C. Afterward, the DMSO was added to the cells (AppliChem; Gatersleben, Germany) and kept in -80°C for an hour.

Measurement of nitric oxide (NO)

Accumulated nitrite, a stable oxidation product of NO, was measured using Griess reagents. 50 µL of primary microglial cell supernatants were transferred to a 96-well microtiter plate, and 50 µL of solution 1 (1% sulfanilamide in 5% phosphoric acid) was

added. After 10 minutes of incubation in the dark, 50 µL of solution 2 (0.1% naphthyl ethylenediamine dihydrochloride) was added and incubated for an additional 10 minutes in the dark. The absorbance was measured at 450 nm using a plate reader (ELISA-Reader Infinite® 200 series, Tecan; Crailsheim, Germany).

Cytokine quantification by ELISA

Microglia cells were collected at different time points. The release of cytokines in the supernatant (TNF-α and IL-6) was measured by using the DuoSet ELISA Development System with mouse TNF-α and IL-6 (e-bioscience; Darmstadt, Germany). The ELISAs were carried out according to the manufacturer's protocol. The initial level of cytokine release (TNF-α and IL-6) was assessed with a single pre-incubation of JN403 (100 nM, 1 µM or 10 µM), and the changes of each cytokine were measured again after human α-synuclein fragment (61-140) on the following day.

Animals

A total number of 30 male C57/BL6N mice (Charles River; Sulzfeld, Germany), 10 weeks old at the beginning of the experiment, were used. The mice were housed in standard cages with *ad libitum* access to food and water at 23ºC with a 12/12 hours light/dark cycle. Animal experiments were performed according to German legislation and mice were handled according to the EU Council Directive 86/609/EEC. Approval of the experiment from the appropriate institutional governmental agency (Regierungspräsidium Giessen, Germany) was documented as V54-19 c 20 15h 01 MR 20/15 Nr. 116/2014.

Targeted WT-αSyn overexpression via the delivery of recombinant AAV5 in the SNc

Mice were deeply anesthetized with a mixture of Ketavet® (100 mg/kg, Zoetis Deutschland GmbH; Berlin, Germany) and 2% Rompun® (5 mg/kg, Bayer; Leverkusen, Germany), diluted in 0.9% NaCl. Later mice were placed in a stereotactic frame (Kopf

Instruments, Tujunga, CA) for surgical procedure [4]. A total amount of 2µl rAAV5-CBA-human-α-synuclein (wild-type; original titer: $1x10^{13}$ vg/ml) or rAAV5-CBA-luciferase (original titer: $1x10^{13}$ vg/ml) was unilaterally injected into the substantia nigra pars compacta (SNc) over ten minutes (flow rate of 200 nl/min) by micro-injection pump (Micro4TM, WPI, Sarasota, USA). After the injection, the needle stayed in the brain for an additional 5 minutes before it was slowly retracted. The injections were performed by using a microsyringe, stainless steel needle (33G, WPI, Sarasota, USA). The coordinates of the injection were anteroposterior: -3.1 mm, mediolateral: -1.2 mm, and dorsoventral: -4.2 mm, relative to bregma using a flat skull position [26].

The viral-mediated vectors were provided by the Michael J. Fox Foundation (https://www.michaeljfox.org/research/research-tools-catalogue.html), and the Gene Therapy Center of the University of North Carolina at Chapel Hill.

The in-vivo experimental design

Mice were habituated for 1 week following arrival. To investigate the effects of JN403 on the wild-type human α-synuclein-induced overexpression in the SNc, animals received the injection of either rAAV5-CBA-human-wildtype-α-synuclein (rAAV-WT-αSyn) or rAAV5-CBA-luciferase (rAAV-luc) (as overexpression of a control protein). Six to eight mice were thereafter assigned to either JN403 treated- or vehicle-treated groups. A total of 4 groups were created; rAAV-WT-αSyn treated with saline (AN), rAAV-WT-αSyn treated with JN403 (AJ); rAAV-luc treated with saline (LN) and rAAV-luc treated with JN403 (LJ).

The dosage of subcutaneous injection (s.c) for JN403 was 30 mg/kg dissolved in saline solution based on the experimental conclusion as previously published [11]. One week after the viral overexpression, mice received a daily subcutaneous injection of JN403 or saline for 9 weeks. Afterward, all mice were sacrificed for further quantification analysis and image processes.

Tissue Preparation and Immunohistochemistry

Tissue preparation and the staining protocols were performed as described

previously [4]. The animals were deeply anesthetized and perfused transcardially with 0.1 M phosphate buffer (PB) followed by ice-cold 4% PFA. Coronal sections of the striatum and the midbrain containing SNc were sliced at 30 µm by a cryostat microtome and collected in 10 regularly spaced series in antifreeze buffer (1:1:3 volume ratio of ethyl glycerol, glycerol, and 0.1 M PB), stored at -20°C before further analysis. After washing with PB buffer 4 times for 5 min each, the sections were then pre-incubated in 5% normal donkey serum and 0.3% Triton X-100 in 0.1 M PB for 30 minutes, and incubated overnight at 4 °C with the primary antibodies [rabbit anti-TH, 1:1000 (Thermo Scientific; Rockford, IL, USA); mouse anti-human α-synuclein 1:1000 (Thermo Scientific; Rockford, IL, USA); goat anti-luciferase 1:5000 (Abcam; Cambridge, UK)]. On the second day, sections were washed and incubated for 1- hour with biotinylated species-specific secondary antibodies [donkey anti-rabbit/-mouse/-goat, 1:1000 (Jackson ImmunoResearch Laboratories Inc.; West Grove, PA, USA)], followed by 1-hour incubation in avidin-biotin-peroxidase solution (ABC Elite, Vector Laboratories; Burlingame, CA, USA). The protein was finally visualized by a 0.1M PB containing 5% 3,3´-diaminobenzidine (DAB) (Serva; Heidelberg, Germany) and 1% H_2O_2. The DAB-stained sections were mounted and counterstained with cresyl-violet and covered by mounting gel with coverslips (Corbit-Balsam; Kiel, Germany).

Double immunofluorescent labeling

The brain sections of the substantia nigra were pre-incubated in 10% normal donkey serum and 0.3% Triton X-100 in 0.1 M PB for 1 hour at room temperature (RT). Then they were incubated overnight at 4 °C with rabbit-anti-TH, 1:1000 (Thermo Scientific; Rockford, IL, USA) and mouse anti-human α-synuclein 1:1000 (Thermo Scientific; Rockford, IL, USA) or goat anti-luciferase 1:250 (Novus Biological; Littleton, CO, USA) primary antibodies followed by washing and incubation with fluorescence labelled donkey anti-rabbit AlexaFluor488 and donkey anti-mouse or goat Cy3 secondary antibodies 1:500 (Jackson ImmunoResearch Laboratories Inc.; West Grove, PA, USA) for 2 hours at RT. For microglia analysis, sheep-anti-TH, 1:1000 (Merck Millipore; Darmstadt, Germany) and rabbit-anti-Iba1, 1:500 (Wako; Osaka, Japan) were incubated overnight. On the next day, the biotinylated anti-rabbit secondary antibody

was used and labeled with anti-goat AlexaFluor488 and AlexaFluor647 Conjugated Streptavidin. All epifluorescence images were acquired using an AxioImager M2 microscope (Carl Zeiss MicroImaging GmbH; Jena, Germany) equipped with an ORCA-Flash4.0 LT Digital CMOS camera (Hamamatsu C11440-42U; Hamamatsu city, Japan).

Unbiased Stereology and Optical density measures

The quantification of TH positive cells was counted by using Stereo Investigator software (v8, MicroBrightField, Magdeburg, Germany) at 40x magnification (Nikon Microphot-FX, Tokyo, Japan). The SNc was outlined as on every 5^{th} serial slice (2.4 to 4.1 mm dorsal of the bregma) and a fractionator probe was established for each section [16]. The criterion for counting an individual TH-ir cell was the presence of its nucleus either within the counting frame or touching the upper and/or right frame lines (green), but not touching the lower and/or left frame lines (red). The number of TH-ir nigral neurons was then determined by the Stereo Investigator program. The entire SNc was delineated from each animal in AN, AJ, LN, and LJ with a method described previously [28].

To quantify the immunoreactivity of reactive microgliosis in the SNc and TH fibers in the striatum, we measured the optical density (OD) of the slices, in comparison with the OD in the injected hemispheres versus the non-injected ones by FIJI software [31]. The striatum was outlined as previously described [3]. The SNc slices were used in the identical anatomical coordinates described in the quantification section; The striatum images were captured from three selected planes: +0.62 mm, +0.5 mm and +0.26 mm relative to bregma, and analyzed using Image J software version 1.43r for Mac OS X platform (http://rsbweb.nih.gov/ij/).

Statistical analysis

All in-vitro experiments were performed with a minimum of three wells per experimental condition. Statistical analysis was performed using the GraphPad Prism 7 (La Jolla, USA). Each data point represents mean ± S.E.M. *$p < 0.05$, **$p < 0.01$, ***p

< 0.001, ****p < 0.0001 compared to control values. Multiple comparisons against a single reference group were performed by one-way ANOVA followed by a posthoc Tukey's multiple comparisons test. For analysis of in-vivo experiments, two-way ANOVA was performed to test the interaction of two variables: protein overexpression and treatment.

RESULTS

Establishment and characterization of αSyn toxicity in-vitro model for evaluation of JN403

To determine whether JN403 elicits any cytotoxic effects in mouse primary microglia cells, we treated microglia cells with three different doses of JN403 (100 nM, 1 µM, and 10 µM) for 24 hours, followed by an assessment of cell viability using the MTT-assay. One-way ANOVA revealed the lack of cytotoxic effects of JN403 in concentrations up to 10 µM, and there was no difference between all these doses [$F_{3, 4} = 1.707$, $p > 0.05$; Fig. 1A]. Based on this data, we decided to use the two lower doses; 100 nM and 1 µM of JN403 for all subsequent in-vitro assays. Next, we verified the αSyn induced toxicity model in this microglia culture in order to provide a platform to examine the effects of JN403 on the inflammatory level. To examine the effect of JN403 in αSyn exposed microglia cell model, we tested the basal toxicity of 1µM of αSyn fragment AA 61-140 (Fig. 1B). Several groups have shown that many types of αSyn fragments have been used in vitro models, but the most toxicity and increased aggregation tendency were observed with C-terminal domains including NAC region of AA 61-95 [8, 21]. Interestingly, we also found that the treatment of 1µM of the αSyn fragment AA 61-140 induced a significant reduction in the number of microglial cells, therefore, it was used to apply in further experiments.

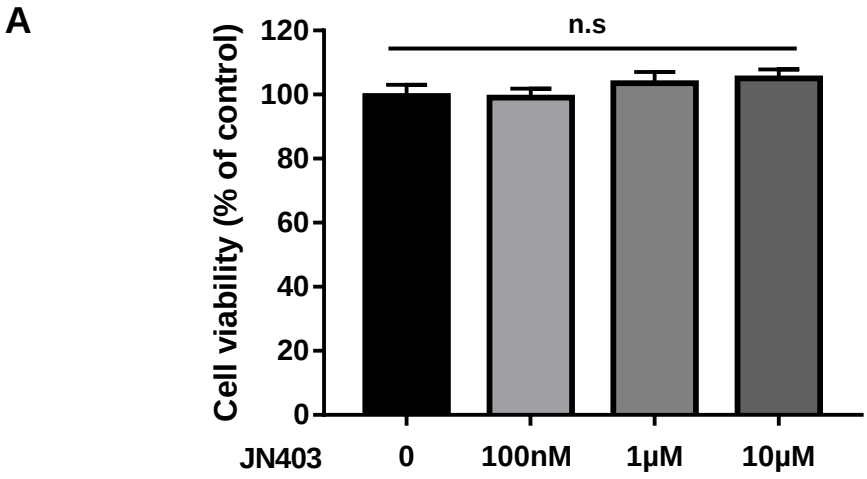

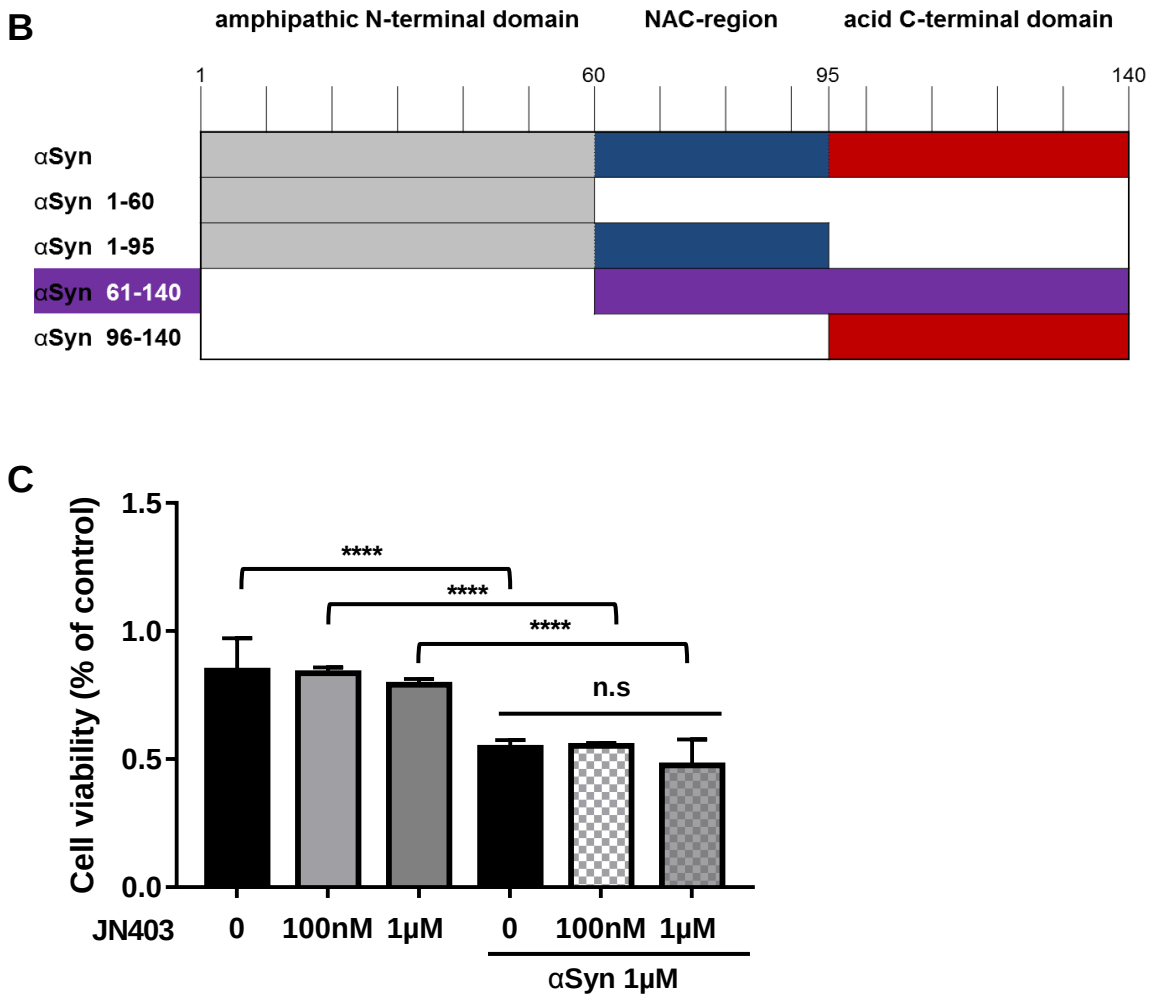

Fig. 1 Microglia cells were incubated with three different doses of JN403 (100 nM, 1 µM, and 10 µM) for 24 hours, followed by an assessment of cell viability using the MTT-assay. (A) JN403 incubation alone, did not elicit cellular toxicity in microglial cells at concentrations up to 1 µM. One-way ANOVA, non-significant (n.s). (B) Overview of αSyn fragment schematic diagram. αSyn fragment 61-140 was only used to induce toxicity for in-vitro experiments. (C) 100 nM or 1 µM of JN403 was pre-incubated with microglia cells, and co-incubated again with 1µM αSyn fragment 61-140 on next day. αSyn treatment induced cytotoxicity in microglial cells, but both 100 nM and 1 µM of JN403 treatment did not affect the cell viability. Data are presented as the mean ± standard error of the mean. Cell viability was measured for multiple independent experiments. **** $p < 0.0001$, significantly different from the control group.

JN403 reduced αSyn induced NO and TNF-α release in microglia cell culture

After performing the evaluation of JN403 concentration in the microglia culture, we selected a parameter, the nitric oxide (NO) release to evaluate the JN403 effects, because NO has been considered as an inflammatory mediator and a neurotoxic effector molecule of immune responses [14, 18]. To elucidate the treatment effect of JN403 on the level of NO changes, microglia cells were pre-incubated with JN403 for 24 hours and co-incubated with 1μM αSyn for another 24 hours. Pre-incubation of 100 nM or 1 μM of JN403 didn't increase NO release, however, we detected that the NO release was increased in all groups when 1 μM αSyn fragment was added [One-way ANOVA, $F_{5, 24} = 276$, (**** $p < 0.0001$); Fig. 2A]. The statistical results showed that both 100 nM and 1μM of JN403 co-incubation significantly decreased αSyn-induced NO release compared to the control without JN403 incubation (100 nM: *** $p < 0.001$, 1 μM: **** $p < 0.0001$ accordingly). The results indicate that JN403 effectively downregulated the NO, in the αSyn model of microglial culture.

Next, changes in the cytokine release, TNF-α and IL-6 were also quantified by ELISA in our microglia model. TNF is known to be essential for the complete expression of inflammation against external microbial invasion, and α7 subunit of nAChRs is known to be required for cholinergic inhibition of TNF release [13, 36, 39]. On the other hands, IL-6 is known to be both pro- and anti-inflammatory cytokine, which can modulate acute or systematic inflammation [30, 41]. Our ELISA results showed that TNF-α level was minimally increased during the pre-incubation of JN403 (100 nM or 1 μM) in microglia cells, but there were no significant differences compared to the control without JN403. When 1μM αSyn was treated, the level of TNF-α was significantly increased [One-way ANOVA, $F_{5, 29} = 89.97$, (**** $p < 0.0001$); Fig. 2B]. However, 100 nM or 1 μM of JN403 co-incubation decreased the TNF-α release compared to the control without JN403 (****$p < 0.0001$). On the other hand, the IL-6 level was also increased when 1μM αSyn was treated [$F_{5, 18} = 24.34$, (**** $p < 0.0001$)] compared to the control without JN403. Neither 100 nM nor 1 μM of JN403 co-incubation altered IL-6 release in microglia cells ($p > 0.05$). To conclude, the results demonstrated that JN403 indeed lowered the pro-inflammatory mediators, especially the NO and TNF-α release, however not IL-6 in this αSyn-induced culture model, implying

a specific role of JN403 to interact with an individual pro-inflammatory cytokine.

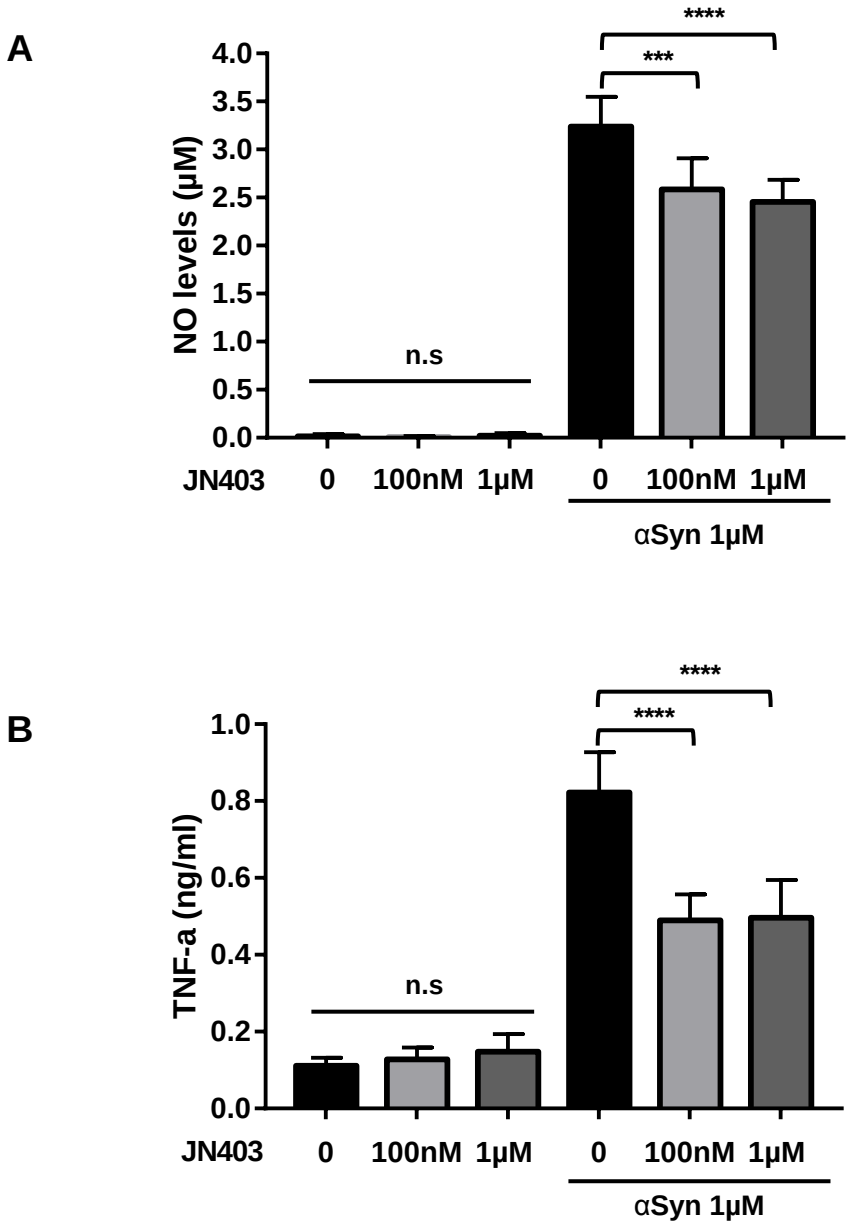

Fig. 2 Inflammatory parameters (A) Nitric Oxide (NO) and (B) TNF-α were measured in JN403 pre-incubated microglia cells for a baseline. (A) NO, and (B) TNF-α release increased with 1μM αSyn treatment, but both 100 nM and 1 μM of JN403 co-incubation significantly reduced NO and TNF-α release One-way ANOVA; * $p < 0.05$, ** $p < 0.01$.

Targeted WT-αSyn overexpression via the delivery of recombinant AAV5 in the substantia nigra compacta (SNc)

To test whether JN403 has the therapeutic effects to ameliorate the toxicity of aSyn or not, we took advantage of recombinant adeno-associated virus (rAAV) harboring human wild-type αSyn (WT-αSyn) genome to create a mouse model of αSyn overexpression in the SNc. The control group received the rAAV-luciferase (luc) to compare to the WT-αSyn overexpression. Stereotaxic microinjection was performed with each vector and three mice per group were selected 3 weeks post-injection to validate the transduction rate [16]. Double immunofluorescence staining against TH/αSyn or TH/luc was conducted in the midbrain areas, and the percentage of dopaminergic cells showing immunoreactivity against human αSyn or luc was calculated. Both rAAVs led to high transduction rates in the dopaminergic SNc neurons of mice, with no significant difference between αSyn and luciferase transduction; 91.7 ± 0.6% for αSyn and 93.4 ± 1.6% for luc. Immunoreactivity of human α-synuclein (hαSyn) was mainly observed in the injected hemisphere 10 weeks post-injection as well (Fig. 3A), and αSyn and luciferase expression were confirmed in the majority of the dopaminergic neurons within the SNc (Fig. 3B-C).

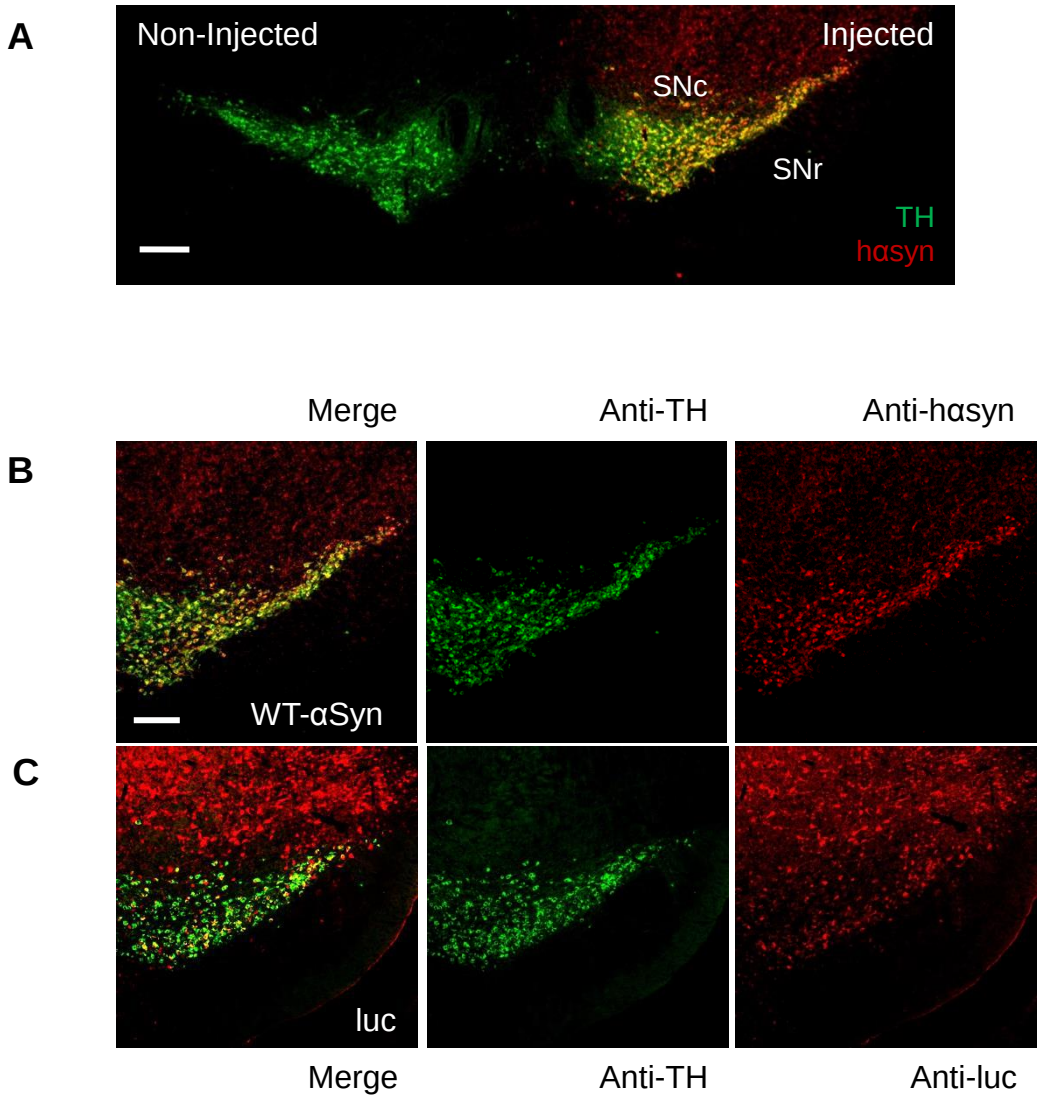

Fig. 3 Double immunofluorescence staining against TH/hαSyn or TH/luc was performed in midbrain slices 10 weeks after the stereotactic microinjection. (A) Merged image of TH (green) and haSyn (red) showed that anti-hαsyn immunoreactivity (ir) is mostly seen in the injected side of substantia nigra compacta (SNc) with rAAV-WT-αSyn. Scale bar = 500 um. (B) Transduction of TH-ir nigral neurons with either rAAV-WT-αSyn or (C) rAAV-luc was confirmed. Anti-TH – green, anti-hαsyn or anti-luc – red. Scale bar = 200 μm.

JN403 did not influence the microglial regulation in the mouse model of WT-αSyn overexpression in the SNc

To explore whether JN403 treatment regulates microglia activation in-vivo after WT-αSyn or luc overexpression in the SNc, we performed double fluorescent staining with Iba1, a microglial marker, and TH. The representative photomicrographs (Iba1 staining) revealed neither an increase in the number nor morphological changes of microglia in the injected side of SNc in both rAAV5-WT-αSyn and luc injected groups [F (1, 12) = 0.03532, (p > 0.05); n=4; Fig. 4A-B]. In addition, the ratio of Iba1-ir density of injected side compared to the non-injected side was analyzed. The results show no significant differences between the rAAV groups and treatment. Two-way ANOVA; n=4, non-significant (n.s).

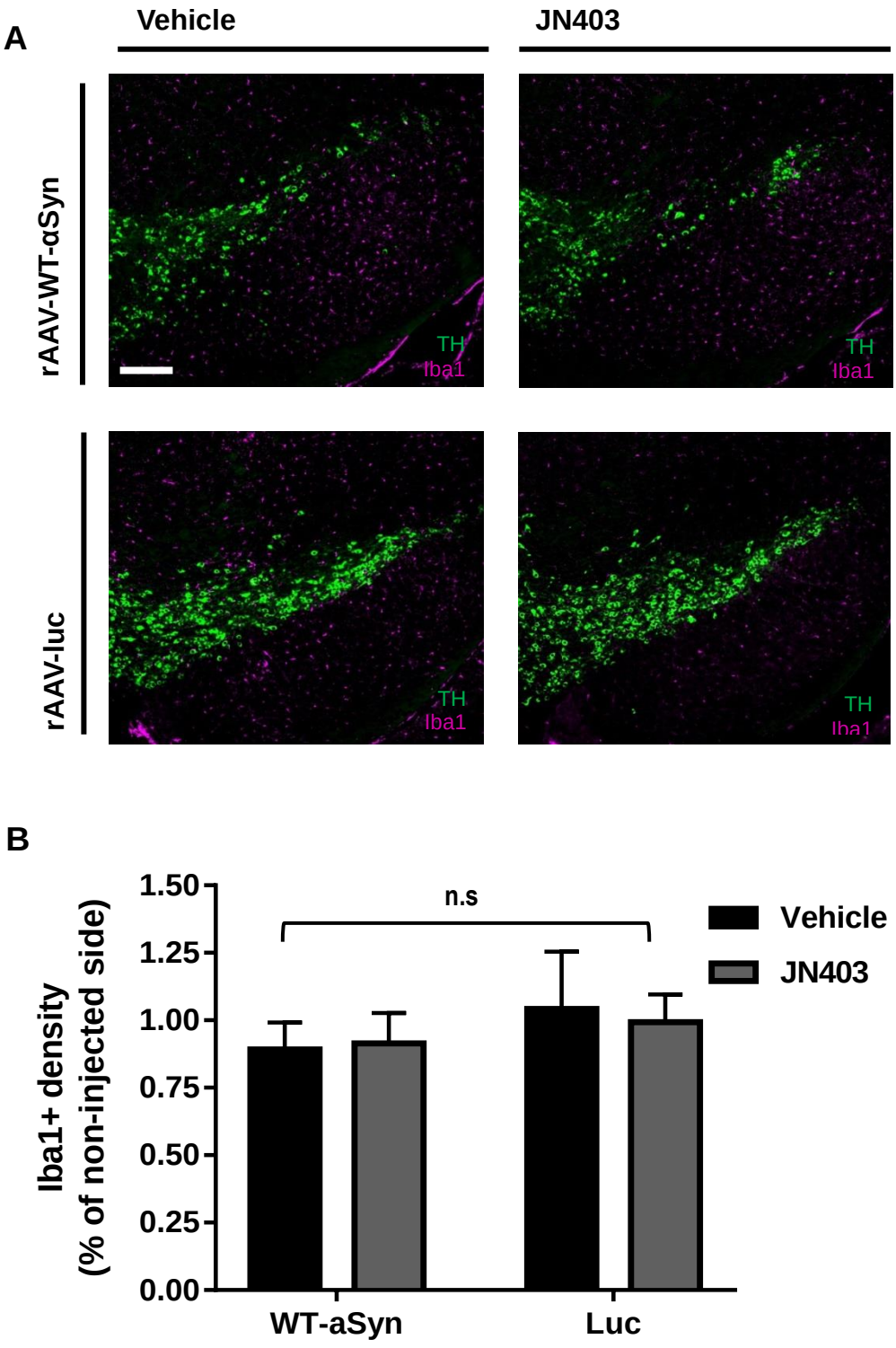

Fig. 4 Iba1-ir microglia cells were detected and the density analysis showed no differences between the rAAV groups and treatment. (A) Representative photomicrographs showing Iba1-ir signals per group, TH (green) and Iba1 (magenta). No activated forms of microglia were found. Scale bar 200 μm. (B) The ratio of Iba-ir density of injected side compared to the non-injected side showed no significant differences between the rAAVs and treatment. Two-way ANOVA; n=4, non-significant (n.s).

Lack of neuroprotective effect of JN403 on the dopaminergic neurons in the mouse model of WT- αSyn overexpression

In order to investigate whether the neuronal loss in the SNc remained unaffected, or there are other biological regulations affected by JN403 in the mouse model of WT-αSyn overexpression, we performed an unbiased, stereological quantification. We found that in vehicle-treated rAAV-luc, the number of TH-ir neurons did not change [4526 ± 195.8 (non-injected) vs. 4440 ± 358.4 (injected side), $p > 0.05$; n=7], also in the group of JN403-treated rAAV-luc, the microinjection did not affect the number of TH-ir neurons significantly [4530 ± 302.6 (non-injected) vs. 4120 ± 358 (injected side), $p > 0.05$; n=6]. In contrast, in the vehicle-treated rAAV-WT-αSyn group the number of TH-ir neurons significantly decreased [4950 ± 212.2 (non-injected) vs. 3930 ± 200.2 (injected side), $p < 0.01$; n=8]. The JN403-treated rAAV-WT-αSyn group also showed significant decline of the number of TH-ir neuron [4563 ± 201.1 (non-injected) vs. 3710 ± 247.2 (injected side), $p < 0.05$; n=8, Fig. 5A]. The number of TH-ir nigral neurons in the injected side was expressed as a percentage compared to that of the non-injected side in all groups. Two-way ANOVA analysis demonstrated that JN403 treatment did not change the number of TH-ir neurons in both rAAV-WT-αSyn and luc injected groups [$F_{1,25} = 0.2556$, ($p > 0.05$)]. A significant difference was only found between rAAVs [$F_{1,25} = 9.068$, (** $p < 0.01$)], as a result, no interaction between the rAAV and treatment factors was found to be significant ($p > 0.05$).

To understand the effect of αSyn and JN403 treatment on the density of dopaminergic terminals, optical density measures of the three selected striatum sections: +0.62 mm, +0.5 mm and +0.26 mm relative to bregma, were analyzed compared to the intact control side after TH staining in each group. The two-way ANOVA result revealed that the striatal density of dopaminergic terminals was significantly reduced in the group of rAAV5-WT-αSyn compared to the luc injected groups [$F_{1, 28} = 4.773$, (*$p < 0.05$); n=7-8, Fig. 6A-B]. However, there was no JN403 treatment effect [$F_{1,28} = 0.029$, ($p > 0.05$)]. Therefore, treatment with JN403 did not influence the mean optical density of TH-ir fibers in the group of rAAV5-WT-αSyn, thus failed to result in a significant difference, when compared to that of the group without JN403 treatment (vehicle).

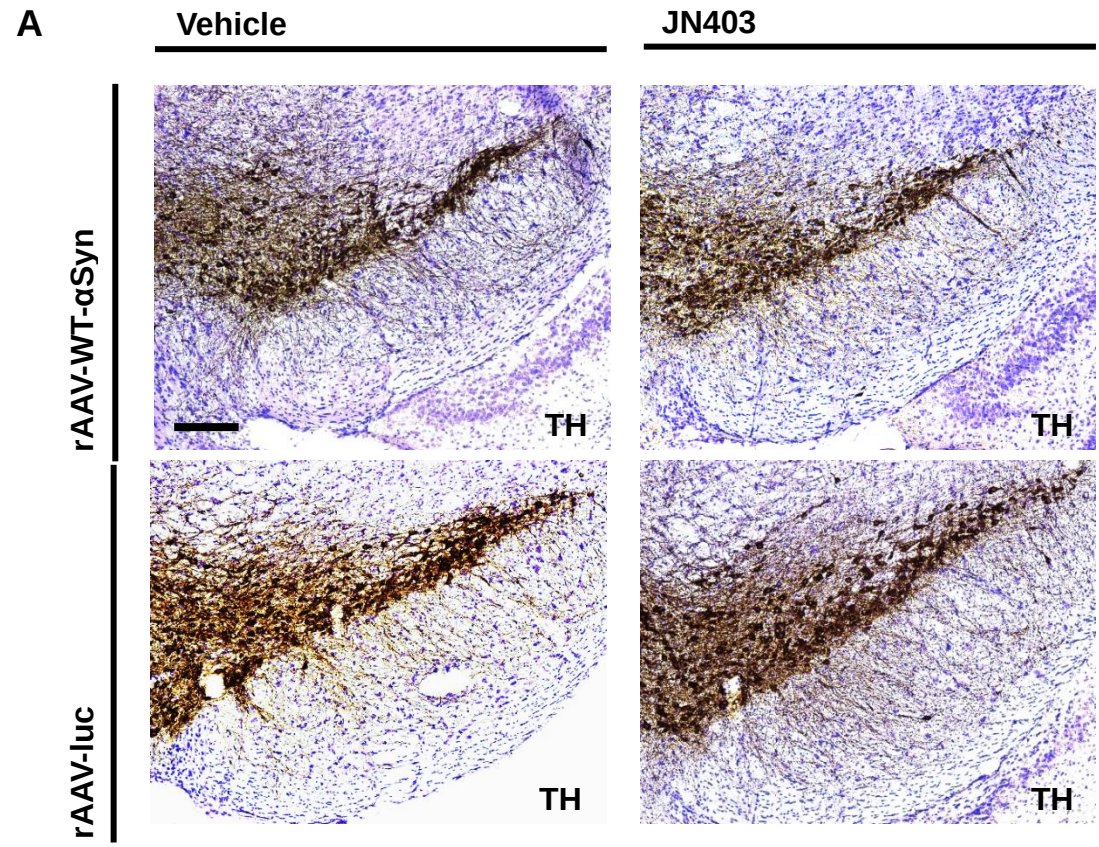

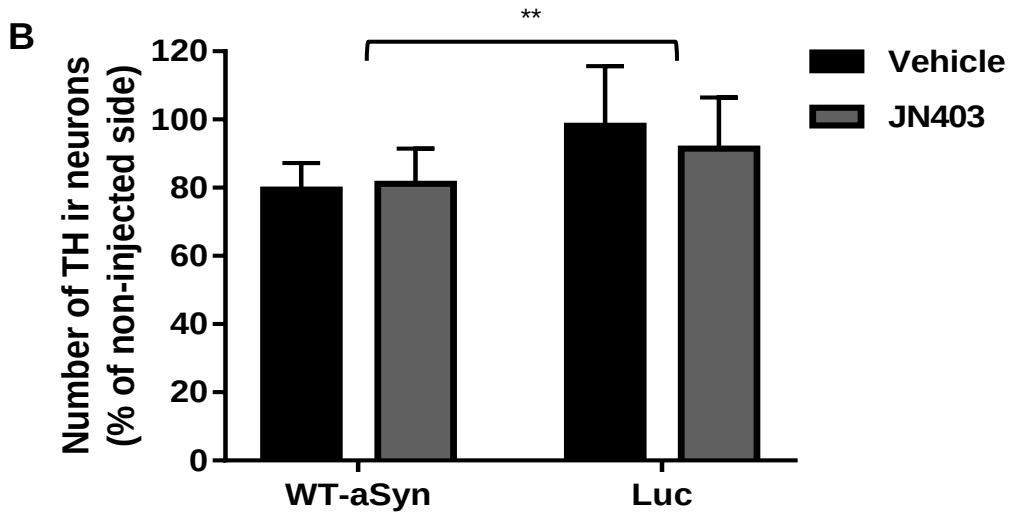

Fig. 5 Stereological analysis of TH-ir neurons in the SN showed no treatment effect of JN403. (A) Representative photomicrographs of TH-ir nigral neurons in each group. Scale bar = 200 μm. (B) Bars in black show non-treated (vehicle) groups and bars in grey show JN403 treated group in either rAAV-WT-αSyn or rAAV-luc injected animals. Percentage of TH-ir nigral neurons in the injected compared to the non-injected side was analyzed; Two-way ANOVA; n=6-8, p ** < 0.01 for rAAV factor; non-significant (n.s) for treatment factor.

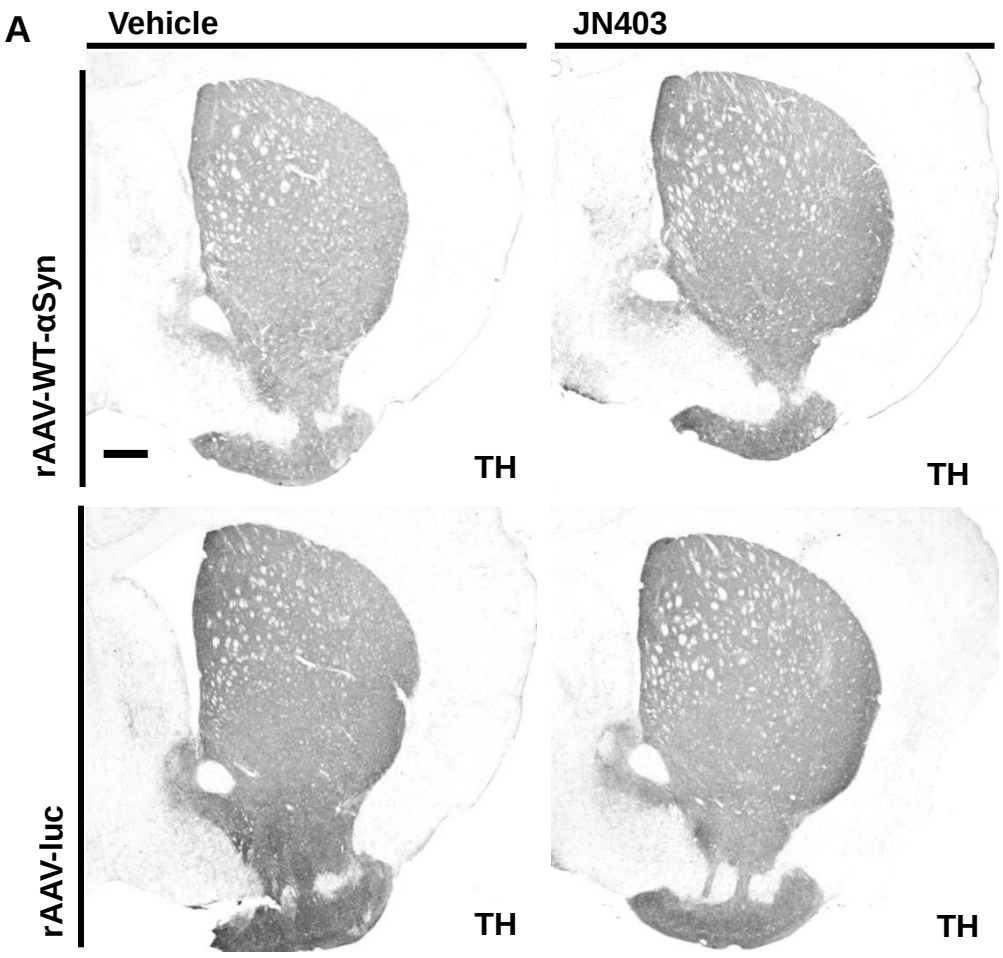
A
Vehicle
JN403
rAAV-WT-αSyn
rAAV-luc
TH
TH
TH
TH

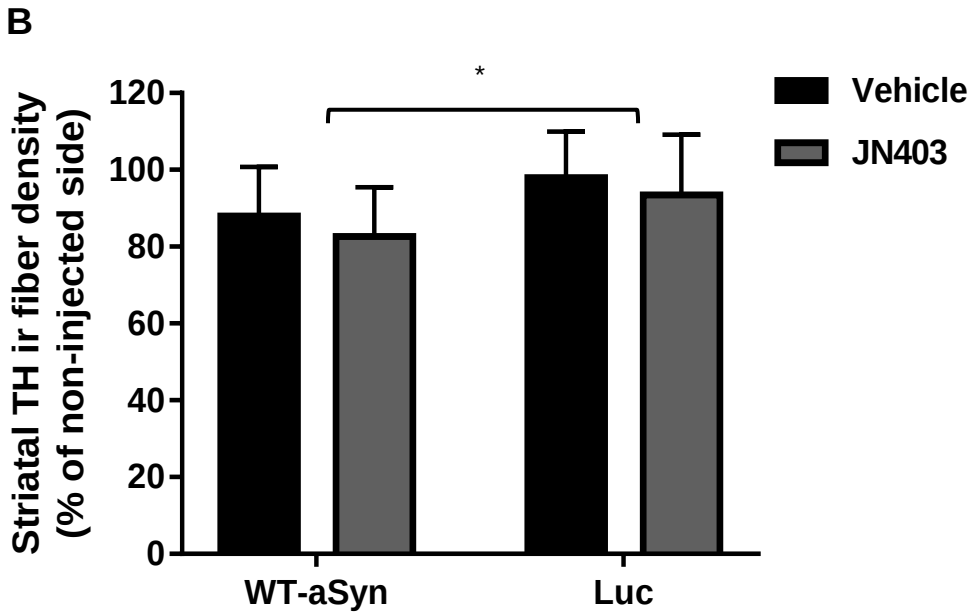
B
Striatal TH ir fiber density
(% of non-injected side)
120
100
80
60
40
20
0
*
Vehicle
JN403
WT-aSyn
Luc

Fig. 6 Striatal TH-ir density analysis showed no treatment effect of JN403. (A) Representative photomicrographs showing the TH-ir fiber in the striatum 10 weeks after either intranigral rAAV-WT-αSyn or luc injection or JN403 treated or vehicle-treated. Scale bar =500 um. (B) Optical density analysis of TH-ir striatal fibers compared to the non-injected side. Bars in black show non-treated (vehicle) and bars in grey show JN403–treated groups in each rAAV-WT-αSyn or rAAV-luc injected animals; Two-way ANOVA; n=7-8, $*p < 0.05$ for rAAV factor.

DISCUSSION

In this study, we investigated the effect of the α7-nAChR agonist, JN403 in in-vitro microglia cell culture exposed to human αSyn and in an in-vivo mouse model of PD using intranigral rAAV5-mediated-WT-αSyn overexpression. Our results in microglia cell cultures reveal that single incubation with αSyn fragment 61-140 induced an increase of Nitric Oxide (NO), TNF-α and IL-6 release, and reduced cell viability. JN403 pre- and co-treatment significantly reduced the release of NO and TNF-α level in microglia cells. In contrast, JN403 treatment showed no effect on IL-6 cytokine release, and cell viability did not increase in this αSyn exposed microglia cell cultures. In addition, in- vivo experiments with targeted nigral overexpression of WT-αSyn via low titer of rAAV in mice showed a mild loss of (about 20%) of TH immunoreactivity, while rAAV-luc did not decrease the number of TH-ir nigral neurons. Chronic daily subcutaneous application of JN403 – starting one week after stereotactic microinjection - did not protect the loss of TH-ir dopaminergic neurons from WT-αSyn-mediated toxicity in this mouse model of PD. These results were consistent with OD analysis from the striatal dopaminergic terminals that JN403 did not revert the reduced TH-ir striatal fibers in the rAAV-WT-αSyn group. In addition, overexpression of WT-αSyn or luc did not induce prominent microgliosis in the SNc, as a result, Iba1-ir microglial density analysis demonstrated no significant differences between all groups regardless of the JN403 administration.

We are aware that it is difficult to relate the experimental design of the microglia culture experiment to a particular stage of Parkinson's disease in the clinic. One may argue that the pre-incubation with JN403 – although only of one 1 day duration - of microglia cultures rather reflected an early (prodromal) stage of PD (exposure of microglia to alpha-synuclein following treatment of the tested compound). The in-vivo experimental design rather reflects the stage of PD when the disease process i.e. alpha-synuclein related pathology starts to affect the SNc (Braak stage 3) before the cardinal PD motor signs manifest [2]. Expression of alpha-synuclein by the focally placed vector started immediately and treatment with the JN403 administration began on the Day 8 following the neurosurgical procedure.

Until now, the evidence on the importance of acetylcholine-mediated reduction in

neuroinflammation has accumulated; enhancing this pathway may be beneficial in the pathogenesis of PD. Murine primary culture microglial cells express the α7-nAChR subunit and microglial TNF-α release was modulated with acetylcholine and nicotine pre-treatment when challenged by lipopolysaccharide (LPS) via activation of α7-nAChR [32]. In fact, targeting the alpha-7 nicotine receptor with partial α7-nAChR agonist, GTS21 showed anti-inflammatory and anti-oxidant effects in an in-vitro model of neuroinflammation using LPS in primary astrocyte cultures [24]. Additionally, α7-nAChR agonist also showed concentration-dependent inhibition of the synthesis and release of proinflammatory mediators, such as IL-1β, TNF-α, IL-6, and HMGB1 from leucocytes by other toxic insults, but generally did not affect anti-inflammatory cytokines, for example, IL-10 [19, 25, 34]. These findings are well in line with our current data in microglial modulation on TNF-α release by the α7-nAChR agonist, JN403 treatment. To our best knowledge, this is the first in-vitro model evaluating this 'cholinergic anti-inflammatory pathway' using human αSyn incubation in microglia cell culture model. Very recently, an animal research using transgenic mice overexpressing human wild-type αSyn under Thy1-promoter (Thy1-aSyn mice) showed that a long-term subcutaneously applied nicotine treatment did not alter αSyn aggregation, nor microglial activation [35]. The nicotine treatment in their study and JN403 in our study used different experimental scheme and mouse models of aSyn. Nevertheless, we propose similar results that both treatments targeting the cholinergic pathway failed to show any neuroprotective effect in ameliorating αSyn pathology in spite of its relatively long- treatment periods.

Our previous work showed a therapeutic effect of the compound PNU-282987 in attenuating dopaminergic neuronal loss in the MPTP toxin-induced mouse model of Parkinson's disease [34]. Interestingly, a recent article demonstrated the therapeutic effect of nicotine using α7-nAChR knockout (a7-KO) mice on MPTP toxin-induced dopaminergic cell loss. As a result, a7-KO mice reversed a beneficial effect of nicotine on the improvement of motor function and of dopaminergic neuronal loss and striatal dopamine release compared to the wild-type littermates [22, 43]. This implies the crucial role of the endogenous α7-nAChR mechanisms in this toxin-induced mouse model of PD. In alignment with all these previous work reporting on the positive effect of α7-nAChR agonist, this in-vivo effect of nicotine was only shown in MPTP-mediated

toxin model. In our previous MPTP model for α7-nAChR agonist investigation, 36 percent of TH-ir nigral neurons was reduced in intoxicated, but saline-treated mice. On the other hand, only 15 percent of TH-ir was reduced in nigral neurons of intoxicated, but PNU-282987 treated mice, although the treatment period was only 6 days. Interestingly, in this toxin-based model with PNU-282987, in-vivo microglia activity was also ameliorated with the treatment on post Day 2 following MPTP intoxication. In contrast, in our current model, the number of TH-ir was reduced about 20 percent after 10 weeks of WT-αSyn overexpression in the nigral neurons. In addition, both WT-αSyn overexpression and the JN403 treatment did not alter microglia activation measured by Iba1-ir signal intensity in the SNc region. These findings and the discrepancy of the treatment effects of α7-nAChR agonists may represent the differences between the toxin-induced model and rAAV mediated model of α-synucleinopathy in mice.

Our results do not exclude the possibilities of potency and pharmacokinetic variances per α7-nAChR agonist in each study. Nevertheless, JN403 showed an anti-inflammatory effect in αSyn induced microglia cells. We recently reported an in-vivo scheme of rAAV5-CBA-mediated WT-αSyn overexpression model via the same titer rAAV delivery in the SNc with Vinpocetine [16]. Thus the human αSyn overexpression model used is – in principle – therapy responsive. Therefore, the reason for this efficacy discrepancy is likely not derived from our experimental design itself but rather relates to the lack of action of JN403 on the rAAV-mediated WT-αSyn overexpression in the SNc. Previous in-vivo characterization study with JN403 in mice demonstrates the brain concentration of JN403 is similar to the compound's EC50 at the nAChR a7 -100 nM, [10] at least 4 h after oral administration of 8.8 mg/kg [11]. In addition, a study with non-human primates reported that the plasma concentration-time profile results of AQW051, another α7-nAChR agonist indicated shorter half-life (~3.5 h with high dose, 15 mg/kg) in cynomolgus monkeys, compared to that of healthy human subjects (19-27 h for young, and 37-46 h for old volunteers) [6]. All these PK differences between humans, monkeys, and mice may help us to understand the lack of effect of JN403 that we observed in our mouse model although a relatively high dose (30 mg/kg) was used. Further well-designed research is necessary to consider evaluating therapeutic compound of the α7-nAChR agonist type in αSyn overexpressed or fibrils mediated in-vivo models, to characterize better the role of α7-nAChR agonists in human αSyn

related models rather than acute toxin models of PD. Moreover, long-lasting nAChR alpha7 activation may be required for clinical efficacy in future translational research of PD.

Part I-6. Summary

(English)

Alpha-7-nicotine-acetylcholine-receptor (α7-nAChR) agonists modulate the cholinergic anti-inflammatory pathway to attenuate proinflammatory signals and reduce dopaminergic neuronal cell loss in toxin-induced experimental murine models of Parkinson's disease (PD). However, no research has been performed to evaluate the effect of α7-nAChR agonists in human α-synuclein (hαSyn) mediated models of PD. We, therefore, investigated the effect of the compound JN403, an α7-nAChR specific agonist, in αSyn treated in-vitro microglia culture and human αSyn overexpression in-vivo mouse model of PD. In primary mouse microglia cells, αSyn fragment 61-140 treatment increased the release of nitric oxide (NO), TNF-α and IL-6, and decreased cell viability. 100 nM of JN403 pre- and co-incubation significantly reduced the level of NO and TNF-α release in the microglial cells. However, cell viability and IL-6 cytokine release did not revert to control level. For in-vivo testing of JN403, unilateral intranigral overexpression of WT-αSyn or of the control protein luciferase (luc) was induced in C57/BL6N mice via stereotaxic delivery of recombinant adeno-associated virus (rAAV) vectors. Targeted WT-αSyn overexpression reduced 20% of the number of tyrosine hydroxylase (TH) immunoreactive (ir) nigral neurons after 10 weeks. Subcutaneous daily treatment of 30 mg/kg JN403 over 9 weeks starting at postoperative week 1 did not reverse the decline of the number of TH-ir nigral neurons (nor Iba1-ir density) in WT-αSyn overexpression mouse model. The reduced density of TH-ir striatal terminals in the WT-αSyn groups was also not recovered by the JN403 treatment. In summary, JN403, an α7-nAChR specific agonist shows a beneficial effect on ameliorating proinflammatory signals in αSyn exposed microglia cells. However, no significant treatment effect is found in an intranigral WT-αSyn overexpression in-vivo mouse model with JN403 therapy employed.

(Deutsch)

Alpha-7-nikotinische Acetylcholin-Rezeptor (α7-nAChR) -Agonisten modulieren den cholinergen anti-inflammatorischen Signalweg, indem sie proinflammatorische Signale abschwächen und den Verlust von dopaminergen Nervenzellen in Toxin-induzierten Mausmodellen der Parkinson-Krankheit (PD) reduzieren. Allerdings fehlen Studien, die die Wirkung von α7-nAChR-Agonisten in PD-Modellen mit humanem Alpha-Synuklein (hαSyn) testen. Wir untersuchten daher die Wirkung des spezifischen α7-nAChR-Agonisten JN403 in-vitro in hαSyn-behandelten Mikroglia-Zellkulturen sowie in-vivo in Mausmodellen mit hαSyn-Überexpression. In den unbehandelten murinen Mikrogliazellen erhöhte die Behandlung mit dem hαSyn-Fragment 61-140 die Freisetzung von Stickstoffmonoxid (NO), TNF-α und IL-6 und verringerte die Viabilität der Zellen. Die Vor- und Ko-Inkubation mit 100 nM JN403 dazu reduzierte die Menge an NO- und TNF-α-Freisetzung in den Mikrogliazellen signifikant. Die Viabilität der Zellen und die IL-6-Freisetzung kehrte jedoch nicht auf das Kontrollniveau zurück. Für das in-vivo Experiment mit JN403 wurde in C57/BL6N-Mäusen eine unilaterale intranigrale Überexpression von WT-αSyn bzw. des Kontrollproteins Luciferase (luc) durch stereotaktische Verabreichung eines rekombinanten adeno-assoziierten Virus (rAAV)-Vektors induziert. Die gezielte WT-αSyn-Überexpression reduzierte nach 10 Wochen 20% der Tyrosinhydroxylase (TH)-immunoreaktiven (ir) nigralen Neurone. Eine tägliche subkutane Behandlung mit 30 mg/kg JN403 über 9 Wochen ab der ersten postoperativen Woche konnte den Verlust der TH-ir nigralen Neurone nicht aufhalten (noch die der Iba1-ir-Dichte). Die reduzierte Dichte von TH-ir striatalen Endigungen in WTαSyn-Gruppen war auch nach JN403-Behandlung unverändert. Zusammenfassend reduzierte der spezifische α7-nAChR-Agonist JN403 proinflammatorische Zytokine in αSyn-exponierten Mikrogliazellen in-vitro, jedoch konnten wir unter der Behandlung mit JN403 keinen signifikanten Effekt im in-vivo Mausmodell mit intranigraler Überexpression von WT-αSyn finden.

1. Ascherio A, Schwarzschild MA (2016) The epidemiology of Parkinson's disease. Risk factors and prevention. Lancet Neurol 15(12): 1257–1272. doi: 10.1016/S1474-4422(16)30230-7
2. Braak H, Del Tredici K, Rüb U et al. (2003) Staging of brain pathology related to sporadic Parkinson's disease. Neurobiol Aging 24(2): 197–211
3. Carlsson T, Schindler FR, Höllerhage M et al. (2011) Systemic administration of neuregulin-1β1 protects dopaminergic neurons in a mouse model of Parkinson's disease. J Neurochem 117(6): 1066–1074. doi: 10.1111/j.1471-4159.2011.07284.x
4. Chiu W-H, Carlsson T, Depboylu C et al. (2014) Selegiline normalizes, while l-DOPA sustains the increased number of dopamine neurons in the olfactory bulb in a 6-OHDA mouse model of Parkinson's disease. Neuropharmacology 79: 212–221. doi: 10.1016/j.neuropharm.2013.11.014
5. de Jonge WJ & Ulloa L (2007) The alpha7 nicotinic acetylcholine receptor as a pharmacological target for inflammation 10(4): 217–224. doi: 10.1038/nrneurol.2014.38
6. Di Paolo T, Grégoire L, Feuerbach D et al. (2014) AQW051, a novel and selective nicotinic acetylcholine receptor α7 partial agonist, reduces l-Dopa-induced dyskinesias and extends the duration of l-Dopa effects in parkinsonian monkeys. Parkinsonism Relat Disord 20(11): 1119–1123. doi: 10.1016/j.parkreldis.2014.05.007
7. Ebersbach G, Stöck M, Müller J et al. (1999) Worsening of motor performance in patients with Parkinson's disease following transdermal nicotine administration. Mov Disord 14(6): 1011–1013
8. El-Agnaf OM, Jakes R, Curran MD et al. (1998) Aggregates from mutant and wild-type alpha-synuclein proteins and NAC peptide induce apoptotic cell death in human neuroblastoma cells by formation of beta-sheet and amyloid-like filaments. FEBS Lett 440(1-2): 71–75
9. Fearnley JM, Lees AJ (1991) Ageing and Parkinson's disease. Substantia nigra regional selectivity. Brain 114 (Pt 5): 2283–2301
10. Feuerbach D, Nozulak J, Lingenhoehl K et al. (2007) JN403, in vitro characterization of a novel nicotinic acetylcholine receptor alpha7 selective agonist.

Neurosci Lett 416(1): 61–65. doi: 10.1016/j.neulet.2007.01.045

11. Feuerbach D, Lingenhoehl K, Olpe H-R et al. (2009) The selective nicotinic acetylcholine receptor alpha7 agonist JN403 is active in animal models of cognition, sensory gating, epilepsy and pain. Neuropharmacology 56(1): 254–263. doi: 10.1016/j.neuropharm.2008.08.025
12. Gerhard A, Pavese N, Hotton G et al. (2006) In vivo imaging of microglial activation with 11C(R)-PK11195 PET in idiopathic Parkinson's disease. Neurobiol Dis 21(2): 404–412. doi: 10.1016/j.nbd.2005.08.002
13. Giebelen IAJ, van Westerloo DJ, Larosa GJ et al. (2007) Local stimulation of alpha7 cholinergic receptors inhibits LPS-induced TNF-alpha release in the mouse lung. Shock 28(6): 700–703. doi: 10.1097/shk.0b013e318054dd89
14. Guzik TJ, Korbut R, Adamek-Guzik T (2003) Nitric oxide and superoxide in inflammation and immune regulation. J Physiol Pharmacol 54(4): 469–487
15. Hirsch EC, Hunot S (2009) Neuroinflammation in Parkinson's disease. A target for neuroprotection? Lancet Neurol 8(4): 382–397. doi: 10.1016/S1474-4422(09)70062-6
16. Höllerhage M, Moebius C, Melms J et al. (2017) Protective efficacy of phosphodiesterase-1 inhibition against alpha-synuclein toxicity revealed by compound screening in LUHMES cells. Sci Rep 7. doi: 10.1038/s41598-017-11664-5
17. Hoover DB (2017) Cholinergic modulation of the immune system presents new approaches for treating inflammation. Pharmacol Ther. doi: 10.1016/j.pharmthera.2017.05.002
18. Jevtović-Todorović V, Todorović SM, Mennerick S et al. (1998) Nitrous oxide (laughing gas) is an NMDA antagonist, neuroprotectant and neurotoxin. Nat Med 4(4): 460–463
19. Kox M, van Velzen JF, Pompe JC et al. (2009) GTS-21 inhibits pro-inflammatory cytokine release independent of the Toll-like receptor stimulated via a transcriptional mechanism involving JAK2 activation. Biochem Pharmacol 78(7): 863–872. doi: 10.1016/j.bcp.2009.06.096
20. Lavedan C (1998) The synuclein family. Genome Res 8(9): 871–880
21. Lee S-b, Park SM, Ahn KJ et al. (2009) Identification of the amino acid sequence

motif of alpha-synuclein responsible for macrophage activation. Biochem Biophys Res Commun 381(1): 39–43. doi: 10.1016/j.bbrc.2009.02.002

22. Liu Y, Hao S, Yang B et al. (2017) Wnt/β-catenin signaling plays an essential role in α7 nicotinic receptor-mediated neuroprotection of dopaminergic neurons in a mouse Parkinson's disease model. Biochem Pharmacol 140: 115–123. doi: 10.1016/j.bcp.2017.05.017
23. Neitemeier S, Jelinek A, Laino V et al. (2017) BID links ferroptosis to mitochondrial cell death pathways. Redox Biol 12: 558–570. doi: 10.1016/j.redox.2017.03.007
24. Patel H, McIntire J, Ryan S et al. (2017) Anti-inflammatory effects of astroglial α7 nicotinic acetylcholine receptors are mediated by inhibition of the NF-κB pathway and activation of the Nrf2 pathway. J Neuroinflammation 14. doi: 10.1186/s12974-017-0967-6
25. Pavlov VA, Ochani M, Yang L-H et al. (2007) Selective alpha7-nicotinic acetylcholine receptor agonist GTS-21 improves survival in murine endotoxemia and severe sepsis. Crit Care Med 35(4): 1139–1144. doi: 10.1097/01.CCM.0000259381.56526.96
26. Paxinos G, Franklin KBJ (2013) Paxinos and Franklin's the mouse brain in stereotaxic coordinates, Fourth edition. Elsevier Academic Press, Amsterdam, Boston, Heidelberg
27. Postuma RB, Anang J, Pelletier A et al. (2017) Caffeine as symptomatic treatment for Parkinson disease (Café-PD). A randomized trial. Neurology 89(17): 1795–1803. doi: 10.1212/WNL.0000000000004568
28. Ries V, Henchcliffe C, Kareva T et al. (2006) Oncoprotein Akt/PKB induces trophic effects in murine models of Parkinson's disease. Proc Natl Acad Sci U S A 103(49): 18757–18762. doi: 10.1073/pnas.0606401103
29. Saura J, Tusell JM, Serratosa J (2003) High-yield isolation of murine microglia by mild trypsinization. Glia 44(3): 183–189. doi: 10.1002/glia.10274
30. Scheller J, Chalaris A, Schmidt-Arras D et al. (2011) The pro- and anti-inflammatory properties of the cytokine interleukin-6. Biochim Biophys Acta 1813(5): 878–888. doi: 10.1016/j.bbamcr.2011.01.034
31. Schindelin J, Arganda-Carreras I, Frise E et al. (2012) Fiji. An open-source

platform for biological-image analysis. Nat Methods 9(7): 676–682. doi: 10.1038/nmeth.2019

32. Shytle RD, Mori T, Townsend K et al. (2004) Cholinergic modulation of microglial activation by alpha 7 nicotinic receptors. J Neurochem 89(2): 337–343. doi: 10.1046/j.1471-4159.2004.02347.x
33. Spillantini MG, Schmidt ML, Lee VM et al. (1997) Alpha-synuclein in Lewy bodies. Nature 388(6645): 839–840. doi: 10.1038/42166
34. Stuckenholz V, Bacher M, Balzer-Geldsetzer M et al. (2013) The α7 nAChR agonist PNU-282987 reduces inflammation and MPTP-induced nigral dopaminergic cell loss in mice. J Parkinsons Dis 3(2): 161–172. doi: 10.3233/JPD-120157
35. Subramaniam SR, Magen I, Bove N et al. (2018) Chronic nicotine improves cognitive and social impairment in mice overexpressing wild type α-synuclein. Neurobiol Dis. doi: 10.1016/j.nbd.2018.05.018
36. Tracey KJ (2002) The inflammatory reflex. Nature 420(6917): 853–859. doi: 10.1038/nature01321
37. Uversky VN (2007) Neuropathology, biochemistry, and biophysics of alpha-synuclein aggregation. J Neurochem 103(1): 17–37. doi: 10.1111/j.1471-4159.2007.04764.x
38. Villafane G, Thiriez C, Audureau E et al. (2017) High-dose transdermal nicotine in Parkinson's disease patients. A randomized, open-label, blinded-endpoint evaluation phase 2 study. Eur J Neurol. doi: 10.1111/ene.13474
39. Wang H, Yu M, Ochani M et al. (2003) Nicotinic acetylcholine receptor alpha7 subunit is an essential regulator of inflammation. Nature 421(6921): 384–388. doi: 10.1038/nature01339
40. Wood H (2017) Parkinson disease. Caffeine and nicotine do not provide symptomatic relief in Parkinson disease. Nat Rev Neurol. doi: 10.1038/nrneurol.2017.155
41. Xing Z, Gauldie J, Cox G et al. (1998) IL-6 is an antiinflammatory cytokine required for controlling local or systemic acute inflammatory responses. J Clin Invest 101(2): 311–320. doi: 10.1172/JCI1368
42. Zhang D, McGregor M, Bordia T et al. (2015) α7 nicotinic receptor agonists reduce

levodopa-induced dyskinesias with severe nigrostriatal damage. Mov Disord 30(14): 1901–1911. doi: 10.1002/mds.26453

43. Zhang Q, Lu Y, Bian H et al. (2017) Activation of the α7 nicotinic receptor promotes lipopolysaccharide-induced conversion of M1 microglia to M2. Am J Transl Res 9(3): 971–985

Alpha-synuclein transfer from noradrenergic locus coeruleus neurons via the vagal motor nuclei to the mouse esophagus: a new prodromal model of Parkinson's disease?

INTRODUCTION

The locus coeruleus (LC), comprising only a few thousand neurons in humans, releases noradrenaline in many anatomically diverse brain regions. The LC neurons play an essential role in a wide range of behavioral and physiological processes including arousal, attention, mood, memory, appetite, and homeostasis [3, 4, 42, 45]. In recent years, aside from these classical roles of the LC, much attention has been paid for the roles in a variety of neurological diseases, such as Alzheimer's disease (AD), Multiple Sclerosis (MS) and Parkinson's disease (PD) [12, 14, 24, 39, 53]. Noradrenaline has been reported to modulate Aβ deposition via microglial functions in an APP-transgenic mouse model of AD [19]. In respect to PD, several experimental studies using mice showed that noradrenaline loss exacerbates MPTP toxin-mediated motor deficits, which suggests that noradrenaline has a protective or compensative role for dopamine functions [30, 39]. In addition, loss of neurons in the LC and the subcoeruleus complex has been implied in prodromal, i.e. premotor symptoms in PD such as rapid eye movement sleep (REM) behavior disorder (RBD). RBD, a sleep-dream-disorder, is the most specific at-risk disorder for PD with a >85% risk to convert to PD, DLB, and MSA and precedes up to several decades the onset of motor symptoms in PD [6, 26, 31]. A recent neuroimaging study demonstrates that a decreased LC neuromelanin signal was found in PD patients with RBD, this was further correlated with impaired cognition and orthostatic hypotension [43].

The LC, as well as the dorsal motor vagus nucleus (DMnX) neurons, are known as vulnerable regions in the early stage of PD [8]. This has been taken as evidence that aggregated pathological alpha-synuclein (αSyn) propagates from the enteric nervous system (ENS) to the cholinergic neurons of the DMnX, then ascend to the locus coeruleus (LC) and the substantia nigra (SN) in a caudo-rostral pattern [8, 17]. In contrast, several animal studies showed that αSyn can also propagate in the opposite direction in a rostro-caudal pattern and within anatomically interconnected regions [29, 38], indicating the heterogeneous pattern of α-synucleinopathies. The DMnX, the nucleus tractus solitarii (NTS), and the nucleus ambiguus (nAmb) belong to the vago-vagal neurocircuit [48]. This circuit has been recognized as the control of the esophagus and the stomach. It is noteworthy that TH-immunoreactive (ir) varicosities on DMnX

and nAmb neurons may originate from the noradrenergic cell group A5 and the LC [44, 52], implying the potential role of the LC in motor innervation of the striated muscle of mouse esophagus.

The importance of developing animal models which help to understand how αSyn aggregates and transmits has been emphasized over years, yet only a limited number of articles are available regarding the noradrenergic neurons in respect to PD. A recent review emphasized that careful consideration must be taken when modeling early PD phenotypes as the patients with an early diagnosis of PD are more driven by an active αSyn pathology that hinders normal cellular functions rather than by overt degeneration [25]. To our knowledge, here we present a novel mouse model resembling the early α-synucleinopathy starting from the LC, and αSyn transfer to the striated muscle and the myenteric plexus neurons of the mouse esophagus via nAmb neurons after only 3 weeks of WT-αSyn overexpression.

METHODS

Viral vectors

In order to overexpress the human wild-type αSyn locally in the LC of mice, we used the recombinant adeno associated viral vectors rAAV1/2-CMV/CBA-human-WT-αSyn or luciferase-WPRE-BGH-pA (Luc) as a control. These viral vectors (titer: $5.1x10^{12}$ VG/ml) were purchased from GeneDetect®, Auckland, New Zealand. Furthermore, in this study, to restrict the expression of WT-αSyn exclusively to the noradrenergic neurons of the LC, we cloned two tyrosine hydroxylase (TH) promoter controlled vectors with human-WT-αSyn AAV2 and the enhanced green fluorescent protein (EGFP) as a control. All the molecular cloning procedures were conducted in SURE2 bacterial cells to minimize the recombination events. Successful AAV2 clones for WT-αSyn or EGFP were transfected with pDG5 plasmid containing AAV5 viral coat proteins into HEK293T (Human Embryonic Kidney) cells. After 48 hours, HEK293T cells were collected to lyse and purify the AAV2/5-TH-WT-αSyn or EGFP particles by further cesium chloride (CsCl) ultracentrifugation, as previously performed [15].

Animals

A total number of 100 male C57/BL6N mice (Charles River, Sulzfeld, Germany), 10 weeks old at the beginning of the experiment, were used. The mice were housed in standard cages with ad libitum access to food and water at 23ºC with a 12/12 hours light/dark cycle. Animal experiments were performed according to German legislation and mice were handled according to the EU Council Directive 86/609/EEC. All experimental procedures were approved by the appropriate institutional governmental agency (Regierungspräsidium Giessen, Germany). Approval of the experiment was provided in the document V54-19 c 20 15h 01 MR 20/15 Nr. 116/2014.

Stereotaxic microinjection

Mice were deeply anesthetized with a mixture of Ketavet® (100 mg/kg; Zoetis Deutschland GmbH, Berlin, Germany) and 2% Rompun® (5 mg/kg; Bayer, Leverkusen, Germany), diluted in 0.9% NaCl. Later mice were placed in a stereotaxic frame (Kopf Instruments, Tujunga, CA) for operation. For the first part of the study, unilateral microinjection of either rAAV-Luc or rAAV-WT-αSyn was performed in the right hemisphere of the LC. For the second part of the study, AAV2/5-TH-EGFP or WT-αSyn was injected targeting the LC in the same way. A total amount of 1.25µl was injected over 10 minutes (flow rate of 125 nl/min) by a micropump (Micro4TM, WPI, Sarasota, USA). After the injection, the needle stayed in the brain for 10 more minutes before it was slowly retracted. All injections were performed using a microsyringe, stainless steel needle (35G, WPI, Sarasota, FL, USA). The coordinates of the injection were anteroposterior: -5.4 mm, mediolateral: -0.9 mm, and dorsoventral: -3.75 mm, relative to Bregma using a flat skull position [35].

Tissue preparation and 3,3-diaminobenzidine (DAB) staining

Tissue preparation and staining procedures were performed as described previously [10]. Transcardial perfusion was performed with 0.1 M phosphate-buffered saline (PBS) solution followed by 4% ice-cold paraformaldehyde (PFA) in 0.1 M phosphate-buffer (PB, pH 7.4) using a supply pump at a rate of 10 ml/min. Brain and esophagus tissues were carefully removed and post-fixed in 4% PFA and then transferred to 30% sucrose solution for cryoprotection. Medulla tissues were cut in 30 µm thick coronal sections and pontine tissues were cut in 20µm thick sections using a cryostat microtome (Leica CM3050 S, Nussloch, Germany). Esophagus tissues were prepared as described previously but cut 30µm thick [52]. Sections were then stored at 4 °C in cryoprotect-solution (1:1:3 volume ratio of ethylenglycol, glycerol, and 0.1 M PB) until further processing. Free-floating sections containing the brainstem regions were prepared for staining with 3,3-diaminobenzidine (DAB) and counterstained with cresyl-violet (Nissl staining) to quantify the immunoreactivity of respective neurotransmitters. Sections were washed in 0.1 M PB and quenched with 3% H_2O_2 and 10% methanol for 15 min. After a second wash, sections were blocked in 5% normal donkey serum with 0.3% Triton X-100 in 0.1 M PB for 1 hour before incubating them overnight with the

respective primary antibodies; rabbit anti-TH (1:1000, Merck Millipore, Darmstadt, Germany); goat anti- ChAT (1:100, Chemicon, Darmstadt, Germany) at 4 °C in the same blocking solution. On the second day, sections were washed in 0.1 M PB solution and then incubated with the appropriate biotinylated secondary antibody for 1 hour followed by incubation in avidin-biotin-peroxidase solution (ABC Elite, Vector Laboratories, Peterborough, UK) for 1 hour before the color reaction was initiated with 5% DAB (Serva, Heidelberg, Germany) diluted in 0.1 M PB solution with 0.02% H_2O_2. All DAB-stained sections were mounted on gelatin-coated glass slides, dried, counterstained with cresyl-violet and finally mounted with Eukitt® (Corbit-Balsam, Kiel-Hassee, Germany). Brightfield images were acquired using an AxioImager M2 microscope (Zeiss, Oberkochen, Germany).

Fluorescent staining

The pontine or medulla sections were initially washed in 0.1 M PB for 20 min, and then pre-incubated in 5% normal donkey serum with 0.3% Triton X-100 in 0.1 M PB for 60 minutes. Rabbit-anti-TH for the pontine and goat anti-ChAT for the medulla tissues were incubated together with mouse anti-human α-synuclein (1:1000, Thermo Scientific, Rockford, IL, USA) or goat anti-luciferase (1:250, Novus Biological, Littleton, CO, USA) overnight at 4 °C, followed by fluorescence labelling with respective secondary antibodies (1:500, Jackson ImmunoResearch Laboratories Inc., West Grove, PA, USA) for 2 hours at room temperature.

For micro-/astroglia analysis, sections were incubated with sheep-anti-TH (1:1000, Merck Millipore, Darmstadt, Germany), rabbit-anti-ionized calcium-binding adaptor protein-1, Iba1 (1:500, Wako, Osaka, Japan) and chicken-anti- glial fibrillary acidic protein, GFAP (1:2000, Abcam, Cambridge, UK) overnight. On the next day, the biotinylated anti-rabbit secondary antibody was used and finally labeled with AlexaFluor647 Conjugated Streptavidin, along with anti-goat AlexaFluor488 and anti-chicken Cy3 respectively.

For the esophageal tissue staining longitudinal cryostat sections of the mouse esophagus were prepared (30μm) and goat-anti-Vesicular Acetylcholine Transporter, VAChT (1:1000, Merck Millipore, Darmstadt, Germany) and α-Bungarotoxin, α-BT-

Alexa Fluor 555 conjugate (1:1000, Molecular Probes, Eugene, OR, USA) were used to stain for motor nerve endings and acetylcholine (ACh) receptors. Vector M.O.M Immunodetection kit (Vector Laboratories, Burlingame, CA, USA) was used with longer incubation time to reduce the endogenous mouse IgG in order to stain esophagus tissues with mouse anti-human α-synuclein. Additionally, rabbit anti-Protein Gene Product 9.5, PGP9.5 (1:1000, Chemicon, Darmstadt, Germany) was used to co-stain the myenteric plexus ganglia and all tissues were mounted using DAPI containing medium (Roti®-Mount FluorCare DAPI, Roth, Karlsruhe, Germany).

Microscopy

All epifluorescence images were acquired using an AxioImager M2 microscope (Zeiss) equipped with an ORCA-Flash4.0 LT Digital CMOS camera (Hamamatsu C11440-42U). For confocal images, the Leica TCS SP8 microscope was used. Epifluorescence and confocal images were processed with FIJI image software to reduce background and enhance signal-to-noise. Image data for 3D reconstructions were obtained with a Zeiss Spinning Disk Microscope (Axio Observer Z1) and post-processed with ZEN 2012 image software (Zeiss).

Stereology

Stereo Investigator software (v11, MicroBrightField, Magdeburg, Germany) at 40x magnification (AxioImager M2 microscope, Zeiss) was used for stereology. In order to determine the extent of loss of LC cells, TH-ir neurons were counted as described [20]. ChAT-ir cells were counted for the DMnX and Namb, and fractionator probe was established for each section per region. The criterion for counting an individual cell was the presence of its nucleus either within the counting frame or touching the upper and/or right frame lines (green), but not touching the lower and/or left frame lines (red). The number of TH or ChAT-ir neurons per region was then determined by the Stereo Investigator program.

Quantification of neuroinflammation

In order to quantify the degree of neuroinflammation signals, we selected 5 representative LC sections per each mouse brain and measured the optical density (OD) of both the injected and the non-injected side using FIJI [41]. First, epifluorescence photographs were converted to 8-bit grey scales and each LC region was outlined with a rectangular contour (1200px x 800px). OD was measured from both hemispheres as well as a partial region from the background to subtract the mean background value for every section. The corrected OD results from all 5 LC sections per hemisphere were summed and the relative percentage of the density signal of the injected side compared to the non-injected control side was calculated accordingly.

Statistical analysis

Statistical analysis was performed using GraphPad Prism 7 (La Jolla, USA). Data are expressed as the percent of corresponding control values. Each data point represents mean ± S.E.M. $*p < 0.05$, $**p < 0.01$ and $****p < 0.0001$ compared to control values. Multiple comparisons were performed by two-way ANOVA followed by a posthoc Tukey's multiple comparisons test. The null hypothesis was rejected at an α risk of 5%.

RESULTS

Moderate loss of TH-ir LC cells after rAAV-WT-αSyn microinjection

Our first set of an experiment aimed at investigating neuronal changes after microinjection of commercially available rAAV-WT-αSyn in the LC. We performed stereotaxic microinjection with rAAV-WT-αSyn or Luc in the LC region and successful transduction was confirmed at Day 3 post-rAAV injection as described previously [20] (Fig.1 A-B). To quantify the neuronal loss after the WT-αSyn or Luc transduction, we performed stereological counting of TH-ir neurons and compared the left side (no injection) and the right side (rAAV injection) in the LC at postoperative weeks 1, 3, 6 and 9. The total number of TH-ir LC neurons in the injected side was expressed as the percentage compared to that of the non-injected side and all groups were analyzed at each time point we selected (Fig.1 C-D). Two-way ANOVA analysis demonstrated that WT-αSyn overexpression induced a moderate, but significant loss of TH-ir LC neurons compared to Luc group [$F(1, 56) = 15.39$, (*** $p < 0.001$)], in a time-dependent manner [$F(3, 56) = 5.822$, (** $p < 0.01$)]. Additional Tukey's multiple comparisons test revealed that in the rAAV-Luc group, the number of TH-ir neurons did not change over 9 weeks, whereas, in the rAAV-WT-αSyn group, cell number was significantly reduced by ≈ 18% starting from 6 weeks when compared to 1week (** $p < 0.01$).

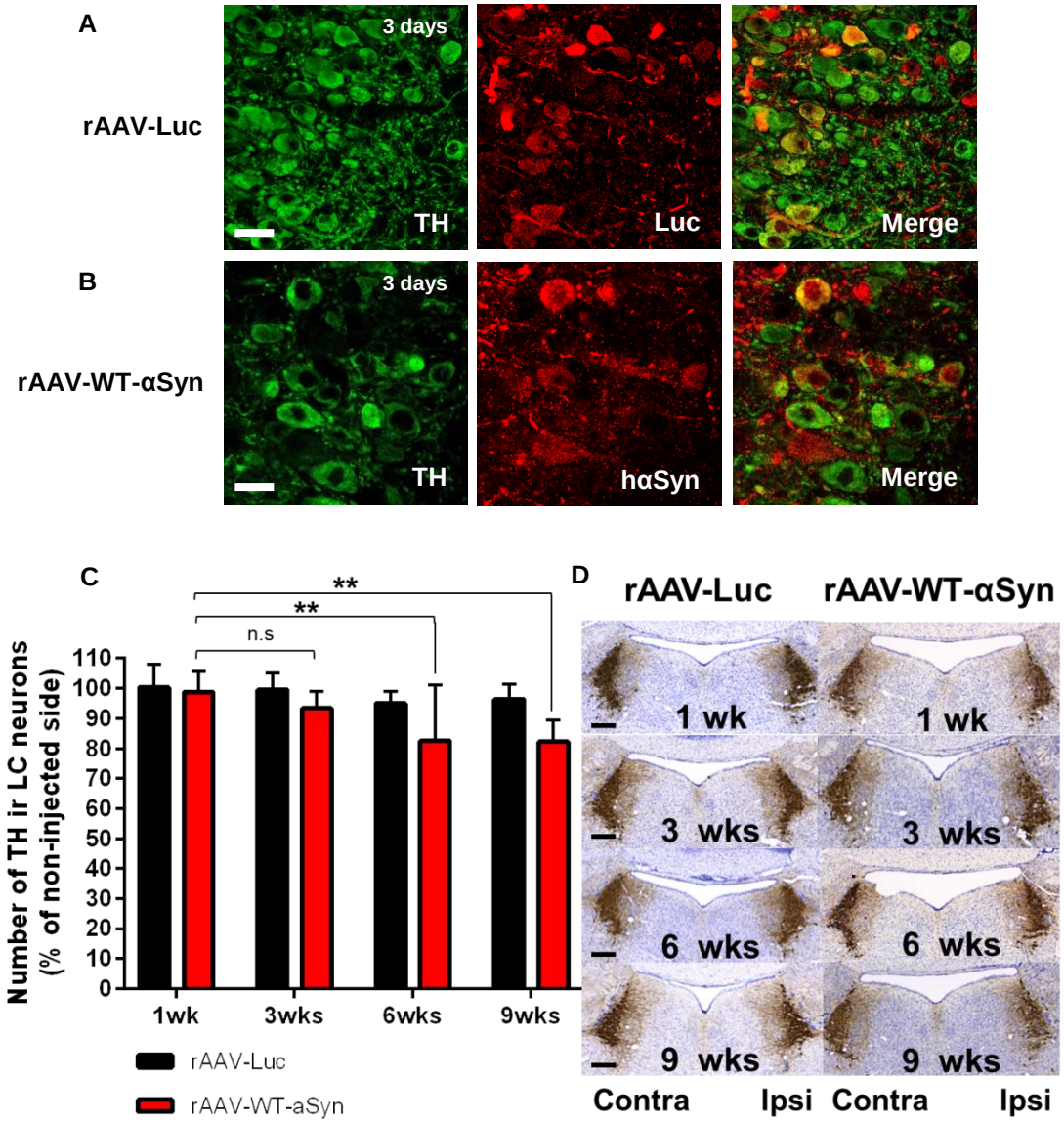

Fig. 1 Moderate loss of TH-ir LC cells after rAAV-WT-αSyn microinjection. (A-B) Overexpression of WT-αSyn or Luc in the mouse LC was performed via unilateral stereotactic delivery of the recombinant adeno-associated viral vectors (rAAV) and transduction was confirmed by immunohistochemistry (n=3). Co-localization of TH (green) with hαSyn or Luc (red) indicates successful protein expression. (C) Unbiased stereology was performed with TH-ir LC neurons of rAAV-WT-αSyn (red bars, right column) or rAAV-Luc (black bars, left column) injected mice. Values (mean ± SEM) are expressed as a relative percentage of the neuronal numbers on the injected side compared to the non-injected side (n=8 per time point and group). Two-way ANOVA analysis followed by Tukey's post-hoc test, (** $p < 0.01$). (D) The

representative images of TH-ir LC neurons were taken at the level of Bregma -5.40 mm in each group, Scale bars: 50 μm (A-B), 250 μm (D).

Early onset of gliosis in the LC region post-WT-αSyn overexpression

To understand temporal aspects of gliosis post-WT-αSyn overexpression in the LC region, we carried out a triple immunofluorescence staining for IbA1, GFAP, and TH, and quantified the increase of fluorescence signals in WT-αSyn or Luc overexpressing animals at postoperative weeks 1, 3, 6 and 9 (Fig.2 A). We measured the relative ratio of a fold increase in the optical density (OD) in the injected side compared to the non-injected side of the LC. Each data set of IbA1 and GFAP was analyzed for the effects of time and rAAV treatment using Two-way ANOVA. The statistical results from both data sets showed a highly significant association for time and rAAV effects (IbA1: [$F(3, 36) = 11.69$, (**** $p < 0.0001$); Fig.2 B] and GFAP: [$F(3, 36) = 13.61$, (**** $p < 0.0001$); Fig.2 C] respectively. As we hypothesized that the activation of glial cells is associated with a reduced number of TH-ir neurons, we further analyzed the onset of gliosis and the activation intensity at each time point. Surprisingly, in the WT-αSyn group, both micro- and astroglia-ir density dramatically increased up to 6-fold as early as 3-weeks post overexpression, being significantly different from that of 1 week (**** $p < 0.0001$), but not statistically different from that of 9 weeks. In addition, abundant reactive forms of astrocytes and microglia were observed near the axon and dendritic sites of the LC neurons. In contrast, only minimal gliosis was observed in the Luc group and Iba1 and GFAP-ir density showed no significant differences over the 9-weeks period accordingly. This may demonstrate that micro-and astroglia became reactive due to αSyn derived from the LC neurons as early as 3 weeks post injection of viral vectors.

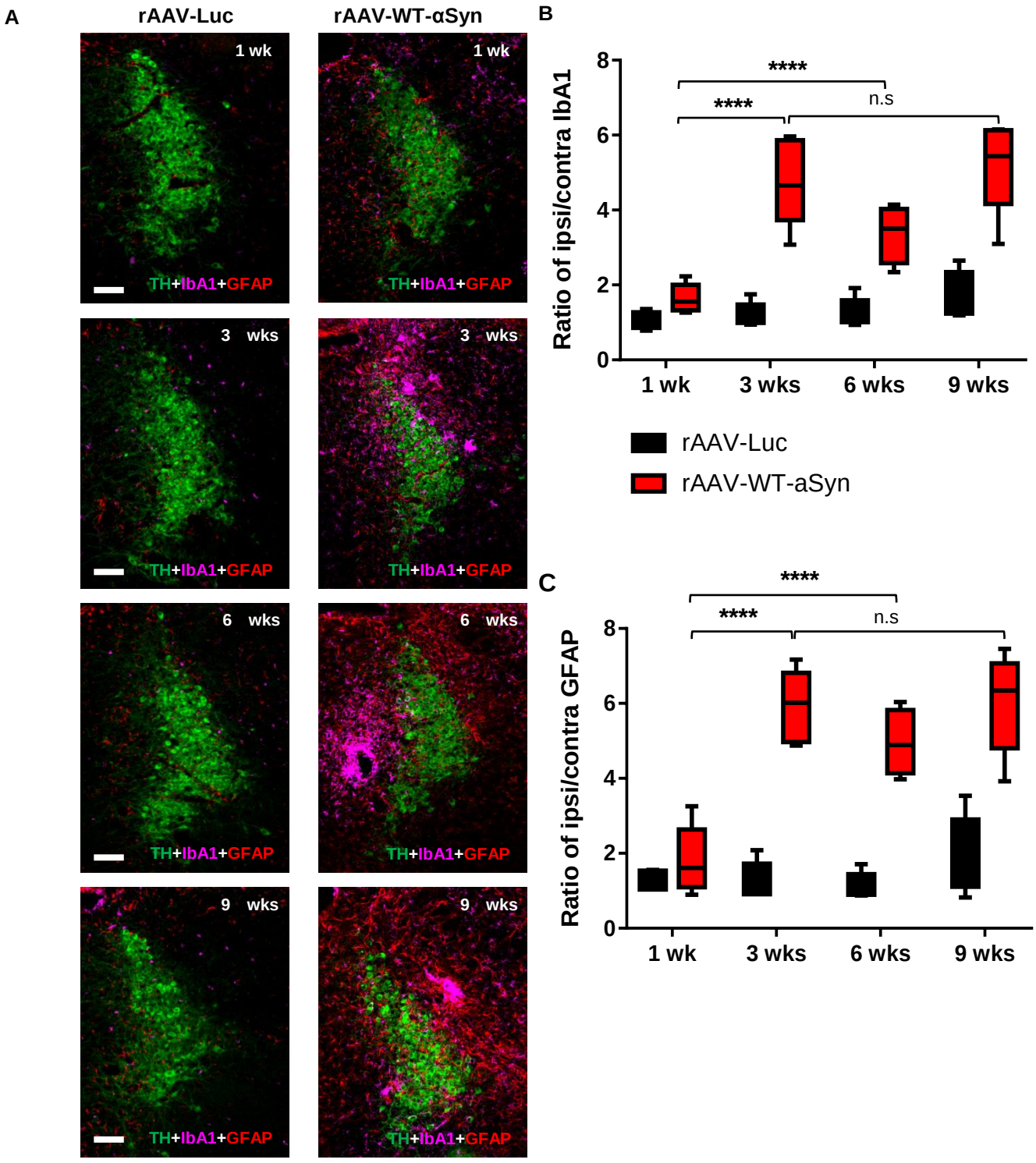
A
rAAV-Luc
rAAV-WT-αSyn
1 wk
3 wks
6 wks
9 wks
TH+IbA1+GFAP
B
Ratio of ipsi/contra IbA1
****
****
n.s
1 wk
3 wks
6 wks
9 wks
rAAV-Luc
rAAV-WT-aSyn
C
Ratio of ipsi/contra GFAP
****
****
n.s
1 wk
3 wks
6 wks
9 wks

Fig. 2 Early onset of gliosis in the LC region post-WT-αSyn overexpression. (A) Representative images of the LC area stained for TH (green), IbA1 (magenta) and GFAP (red) showing a marked increase of micro- and astroglia as early as 3 weeks post the WT-αSyn overexpression. Quantification of IbA1 (B) and GFAP (C) signal intensity revealed a prominent increase of micro- and astroglia in rAAV-WT-αSyn injected mice (red bars) compared to Luc injected mice (black bars). Values (mean ± SEM) are expressed as the signal intensity ratio of the injected side compared to the non-injected side. n = 6 animals per time point and group. Two-way ANOVA analysis revealed a highly significant association for the rAAV factor and for a time factor in both IbA1 and GFAP optical density (OD) analysis (**** $p < 0.0001$). Further, Tukey's post-hoc test results show that the early onset of micro-astrogliosis at 3 weeks was not significantly different from the results of 9 weeks ($p > 0.05$). Scale bars: 100 µm.

Loss of ChAT-ir DMnX neurons post-WT-αSyn overexpression in the LC

A recent review emphasized that synaptic and neuronal transfer of αSyn between vulnerable nerve cells is crucial in the pathogenesis of sporadic PD [7]. Therefore we aimed at investigating other vulnerable neurons, namely the vagal motor nuclei, after the unilateral αSyn overexpression in the LC. First, we quantified ChAT-ir neurons in the DMnX including two regions; the intermediate (at the level of the area postrema, AP) and the rostral (at the level of the 4^{th} ventricle) parts. ChAT-ir DMnX neurons in both hemispheres were quantified for each group post 3 and 9 weeks. Interestingly, WT-αSyn overexpression in the LC significantly decreased the number of ChAT-ir neurons of the DMnX in the ipsilateral part only after 3 weeks (Fig.3 A-B). Two-way ANOVA demonstrates that WT-αSyn overexpression significantly influenced the number of ChAT-ir neurons [$F(1, 19) = 13.44$, ($^{**}p < 0.01$)]. Additionally, Tukey's multiple comparisons test revealed that the reduced number of ChAT ir DMnX in the ipsilateral was statistically different compared to that of rAAV-Luc groups [($^{**}p < 0.01$); Fig.3 C]. Next, we checked how these neurons in the DMnX were changed after 9 weeks of WT-αSyn overexpression in the LC (Fig.3 D-E). The attenuation of ChAT immunoreactivity was sustained in the DMnX 9 weeks after WT-αSyn overexpression as well [$F(1, 22) = 9.565$, ($^{**}p < 0.01$); Fig 3 F]. These findings imply that WT-αSyn unilaterally overexpressed in the LC potentially decreased ChAT immunoreactivity of the DMnX neurons. The number of TH-ir LC neurons did not decrease within 3 weeks of overexpression, yet, ipsilateral sides of DMnX neurons showed a significant decline in ChAT-ir cells at this time point although they were not directly transduced with αSyn.

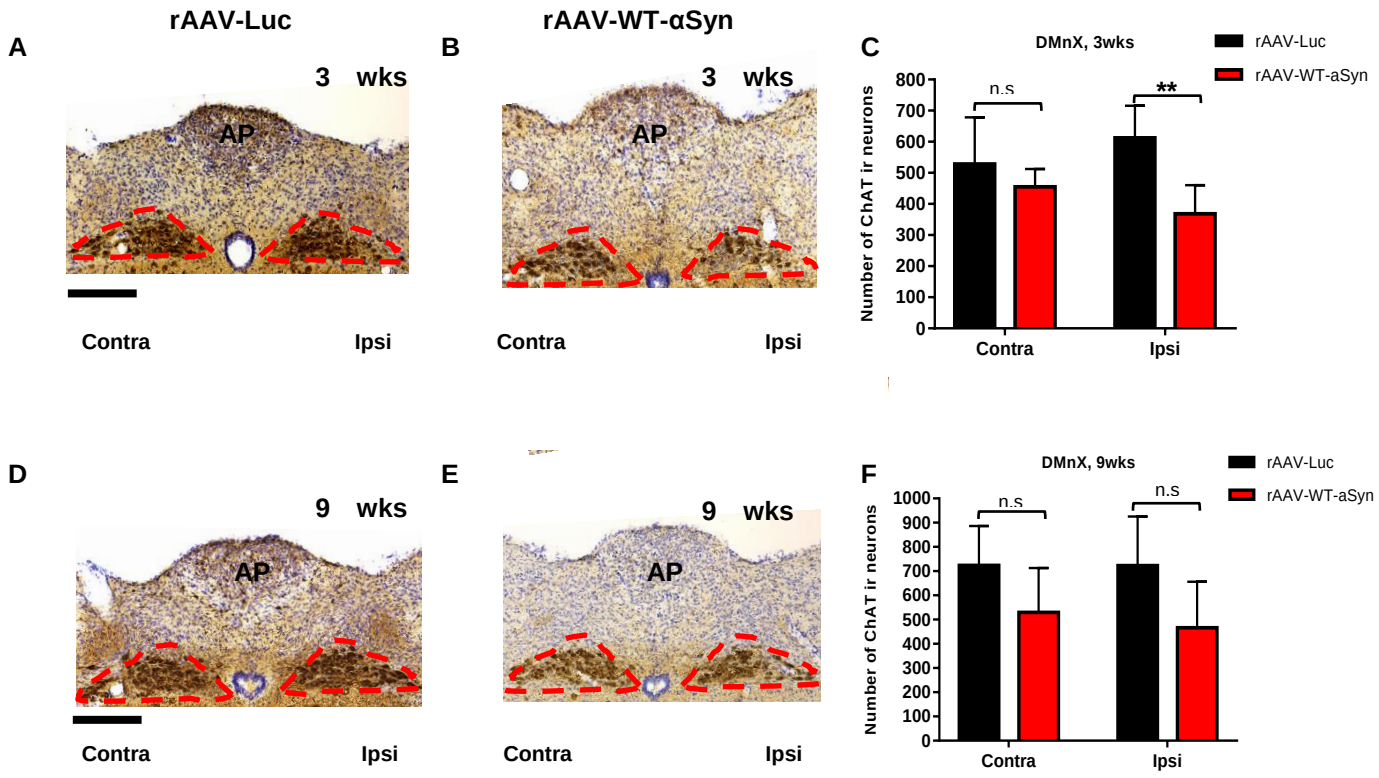

Fig. 3 Loss of ChAT-ir DMnX neurons post-WT-αSyn overexpression in the LC. Representative images of the DMnX area, (A-B, D-E) for the intermediate level stained for ChAT post 3 and 9 weeks of the rAAV-WT-αSyn or Luc overexpression in the LC respectively. (C) Stereological quantification of ChAT-ir DMnX neurons in both contra and ipsilateral side to the LC injection were quantified, and the number in rAAV-WT-αSyn (red bars) was compared to control values in the rAAV-Luc groups (n=5-6). Two-way ANOVA analysis revealed that the rAAV-WT-αSyn significantly changed the number of ChAT ir neurons in both post 3 and 9 weeks compared to rAAV-Luc groups (**$p < 0.01$). However, additional Tukey's multiple comparisons test revealed that only the ipsilateral side of ChAT-ir DMnX neurons in the rAAV-WT-αSyn after 3 weeks showed statistical significance. *Scale bars:* 200 µm.

Loss of ChAT-ir ambiguus neurons post-WT-αSyn overexpression in the LC

To determine if the other vagal motor nucleus, the nAmb, was also influenced by WT-αSyn-transduced LC neurons or not, ChAT-ir compact and semi-compact formation ambiguus neurons were selected and quantified (-7.1mm and -7.48mm relative to bregma) [35]. The number of ChAT-ir ambiguus neurons in both hemispheres were estimated via stereological counting and analyzed in the same way as described above for the DMnX neurons. Two-way ANOVA analysis demonstrates that WT-αSyn overexpression decreased the number of ChAT ir neurons in the nucleus ambiguus compared to the control value in the Luc group at 3 weeks post injection in the LC [$F(1, 20) = 7.886$, ($*p < 0.05$); Fig.4 A-C], and as well at 9 weeks post-injection [$F(1, 14) = 28.03$, ($***p < 0.000$); Fig.4 D-F]. As the nAmb neurons in both hemispheres decreased their immunoreactivity post 9 weeks, there was no statistically significant difference between the contra and ipsilateral sides in the rAAV-WT-αSyn group ($p > 0.05$). Based on these outcomes, we assumed a closely interconnected anatomical relationship between the LC and the nAmb; however, we wanted to interpret with caution in our current model as the 4^{th} ventricle and adjacent nuclei, i.e. parabrachial nuclei, were also transduced when rAAV- mediated WT-αSyn was delivered in the unilateral side of the LC. Therefore, we designed a new set of experiments to confirm these findings.

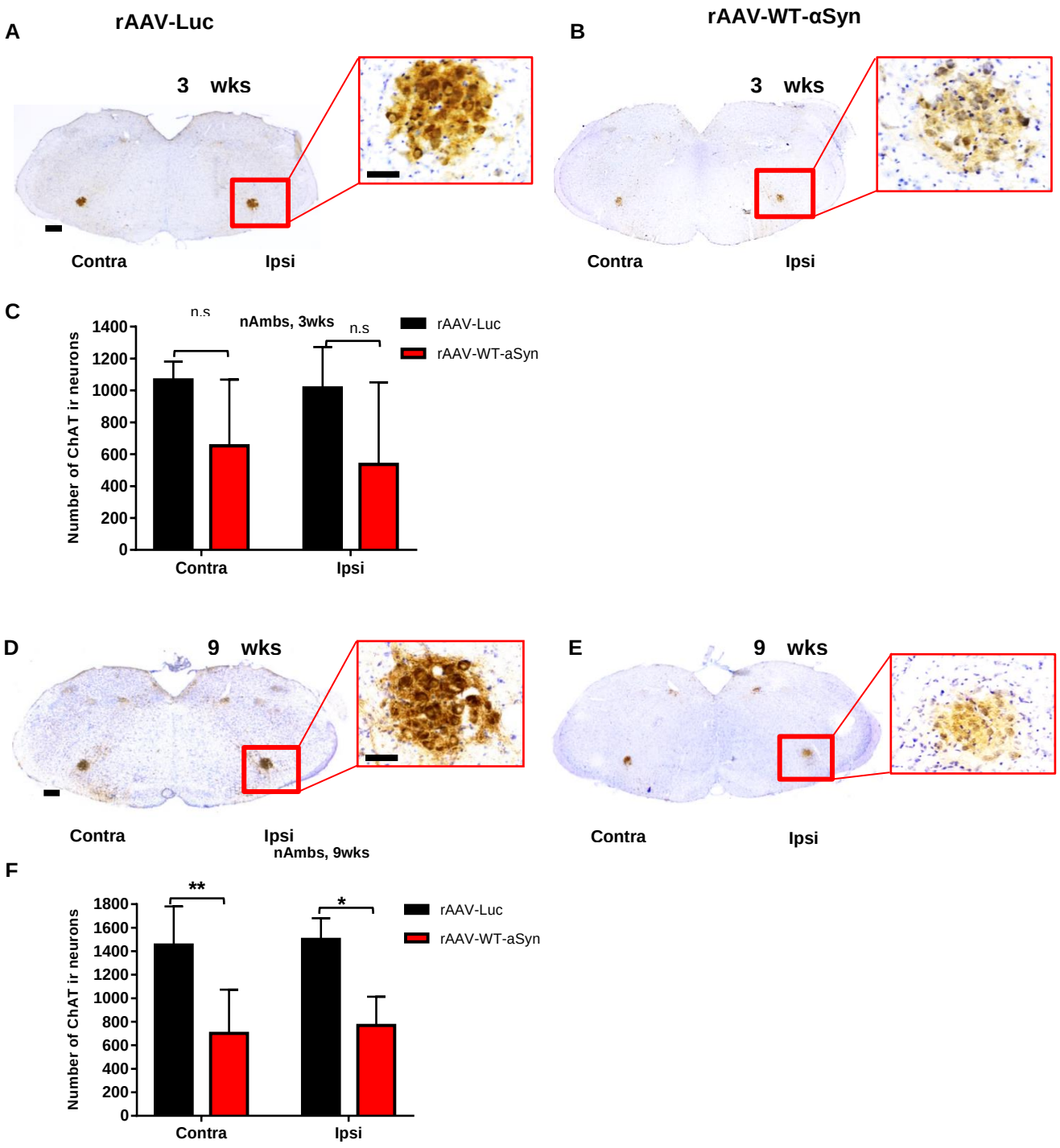

Fig. 4 Loss of ChAT-ir ambiguus neurons post-WT-αSyn overexpression in the LC. Representative images of the compact formation of the nAmb (A-B and D-E), stained for ChAT post 3 and 9 weeks of the rAAV-WT-αSyn or Luc overexpression in the LC respectively. (C) Stereological quantification of ChAT-ir ambiguus neurons in both contra and ipsilateral side to the LC injection was performed and the cell number in rAAV-WT-αSyn injected animals (red bars) was compared to control values in the rAAV-Luc groups (black bars) post 3 and 9 weeks

(n=5-7). Two-way ANOVA analysis showed that αSyn overexpression in the LC significantly changed the number of ambiguus neurons both post 3 and 9 weeks (*$p < 0.05$ and ***$p < 0.001$ respectively). Tukey's correction revealed that the number of ChAT-ir ambiguus neurons decreased in both hemispheres post 9 weeks, *$p < 0.05$, **$p < 0.01$. *Scale bars:* 500 µm (lower magnification), 50 µm for (higher magnification).

AAV2/5-TH-promoter-dependent WT-αSyn overexpression in the LC confirms synaptic transport of αSyn to vagal motor nuclei

In order to further elucidate whether the loss of ChAT expression in the vagal motor nuclei was solely caused by LC neurons-derived αSyn or not, we designed a second set of experiments. We generated a recombinant AAV2/5-TH- viral vector delivering either EGFP or WT-αSyn to achieve a strictly confined protein overexpression in the LC (Fig.5 A). The unilateral side of the LC was targeted using this neurotransmitter specific virus with the same stereotactic approach as performed in the first set. A transfection rate of ≈ 98% was confirmed 3 weeks post-viral vector delivery per group (n=3), and EGFP or WT-αSyn transduction was nearly only detectable within the LC (Fig. 5 B).

We selected two different time points, 3 and 9 weeks, post rAAV2/5-TH-EGFP or WT-αSyn injection into the LC to investigate any transsynaptic or transneuronal αSyn signals in the vagal motor nuclei. We performed fluorescent staining against αSyn with medulla tissues to verify if the reduced number of ChAT-ir neurons in the vagal motor nuclei were due to αSyn transport or not. As a result, we observed that the NTS, the DMnX, and the AP area showed αSyn-ir axon varicosities as early as 3 weeks post-injection (Fig.5 C). We further divided the DMnX into the rostral and the intermediate parts and observed these structures in 3-dimensional image stacks to understand better their structure and physical proximity. This approach revealed that DMnX neurons in both hemispheres were surrounded by αSyn-ir axons at both 3 and 9 weeks post the microinjection (Fig.5 D-E). In addition, we also found that the compact formations of ambiguus neurons were engulfed by αSyn-ir varicosities as well as early as 3 weeks post the injection (Fig.5 F). Remarkably, intraneuronal αSyn was detected in the ambiguus neurons of both hemispheres 3 and 9 weeks post the injection, and these structures were distinguished from αSyn-ir axons around the DMnX neurons (Fig.5 G-H). Intracellular αSyn was present in virtually most of the compact formation of nAmb as a result of the rAAV2/5-TH-WT-αSyn injection in the LC, and it was accompanied with severely weakened ChAT-immunoreactivity as also observed previously in the first set of experiments (n=10). The expression of αSyn in the vagal nuclei was negative in all the medulla tissues in the rAAV2/5-TH-EGFP groups (data not shown).

Part 1I-4. Results

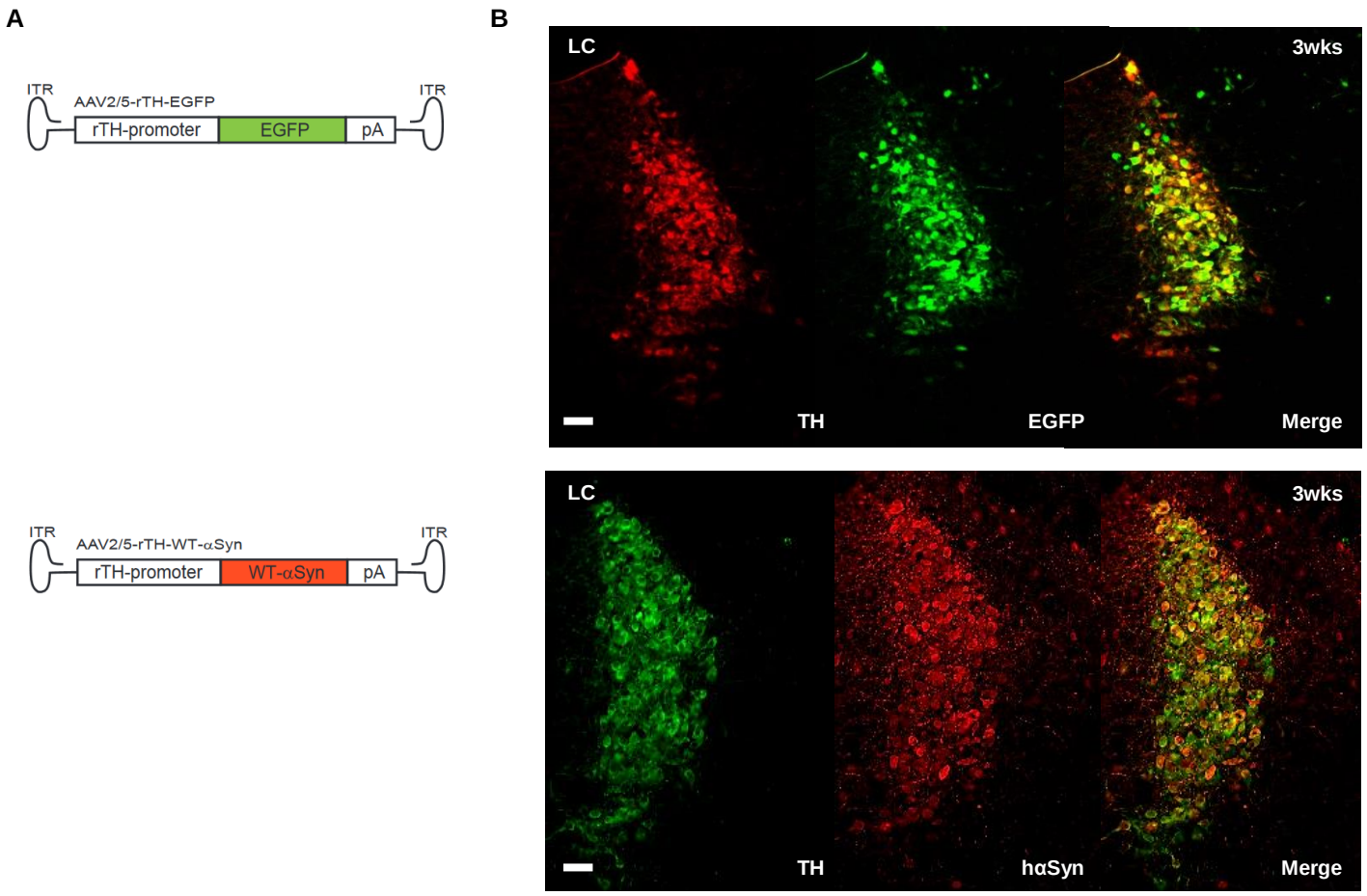

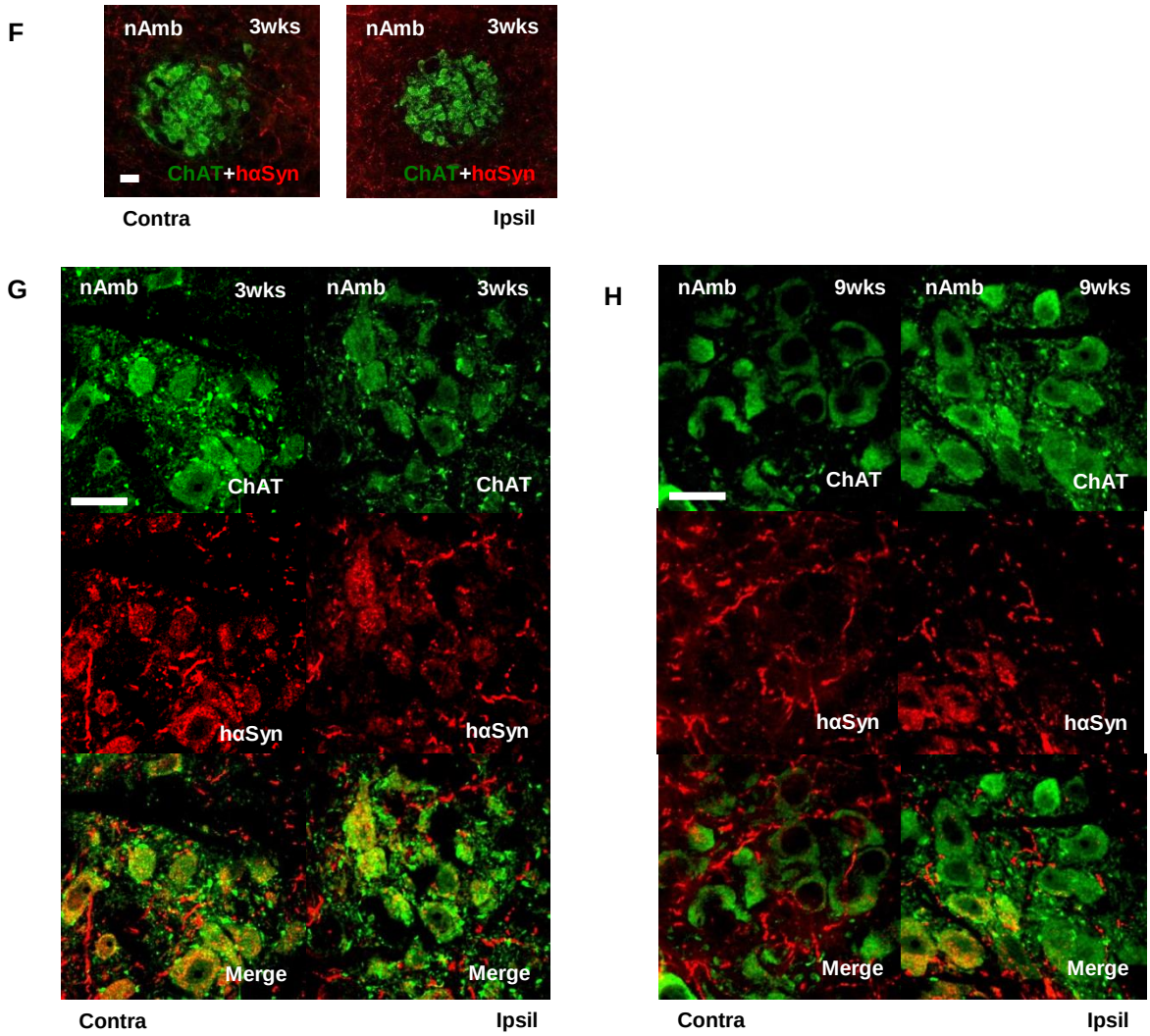

Fig. 5 AAV2/5-TH-WT-αSyn overexpression in the LC confirms synaptic transport from the LC to the vagal motor nuclei. (A) Cartoons displaying the AAV2/5-TH-EGFP or WT-αSyn viral genome. (B) Representative epifluorescent images of immunohistochemical staining following 3 weeks post AAV2/5-TH-EGFP or WT-αSyn microinjection in the LC of the right hemisphere. The noradrenergic TH-ir neurons were marked in (red) in AAV2/5-TH-EGFP, and (green) in AAV2/5-TH-WT-αSyn. The LC neurons ir against EGFP are labeled in (green), human αSyn are labeled in (red), and colocalization is indicated by a yellow merge. (C) Overview of a medulla brain section containing the DMnX, NTS, and AP immunolabeled for ChAT in (green) and αSyn in (red) 3 weeks post the injection. (D-E) The representative 3D stack images of the rostral and the intermediate DMnX clearly show close contact of αSyn-ir axons with cholinergic motor neurons in both hemispheres following 3 and 9 weeks post the injection. (F) Overview of the compact formation of the contra and the ipsilateral nAmb immunolabeled for ChAT in (green)

and αSyn in (red) 3 weeks post the injection. (G-H) The representative images from the stack of the nAmbs demonstrate intracellular αSyn in both contra and ipsilateral sides as early as 3 weeks post-injection, and this αSyn expression was sustained until 9 weeks. *Scale bar* 100 µm (B and F), 200 µm (C), 50 µm (D, E, G, H).

αSyn transport to the cervical, thoracic and abdominal parts of the mouse esophagus.

From our two sets of experiments, we observed a significant decrease of ChAT-ir neurons in the DMnX with prominent αSyn-ir varicosities, and even a more severe decline of the ChAT-ir neuronal numbers in the nAmbs with intraneuronal αSyn after LC microinjection. These outcomes raised the intriguing question of whether αSyn overexpression in the LC might influence the gastrointestinal area that is controlled by the vagal nuclei? In rodents, the esophageal muscle is only composed of striated fibers and is therefore controlled by motoneurons, especially by the compact formation of the nAmb [22, 23, 56]. We, therefore, prepared longitudinal sections of the cervical, thoracic and the abdominal parts of the whole esophagus after the recombinant AAV2/5-TH-EGFP or WT-αSyn microinjection in the LC to investigate αSyn transport and relevant neurochemical changes in these regions.

We performed immunohistochemistry to detect αSyn, and co-immunolabelings with VAChT or PGP 9.5 to further identify the vagal motor nerve endings or myenteric ganglia within the mouse esophagus. Interestingly, we observed no αSyn-ir expression in the rAAV2/5-TH-EGFP group (Fig.6 A) but found various types of αSyn-ir structures depending on the muscle layers, and αSyn-ir enteric neurons were identified within the cervical, thoracic and the abdominal (lower sphincter) of the esophagus after 3 and 9 weeks post the microinjection (Fig.6 B-D). We also examined the motor endplates in each section of the esophagus to elucidate if the motor endplates are in close contact with αSyn or not. As a result, we found αSyn-ir vagal motor endings in the thoracic segments of the esophagus after 9 weeks of overexpression (Fig.6 E). The αSyn signal was intense and it completely co-localized with vagal motor nerve endings. These findings seemed to be highly associated with the intracellular αSyn in the nAmb neurons that we observed earlier.

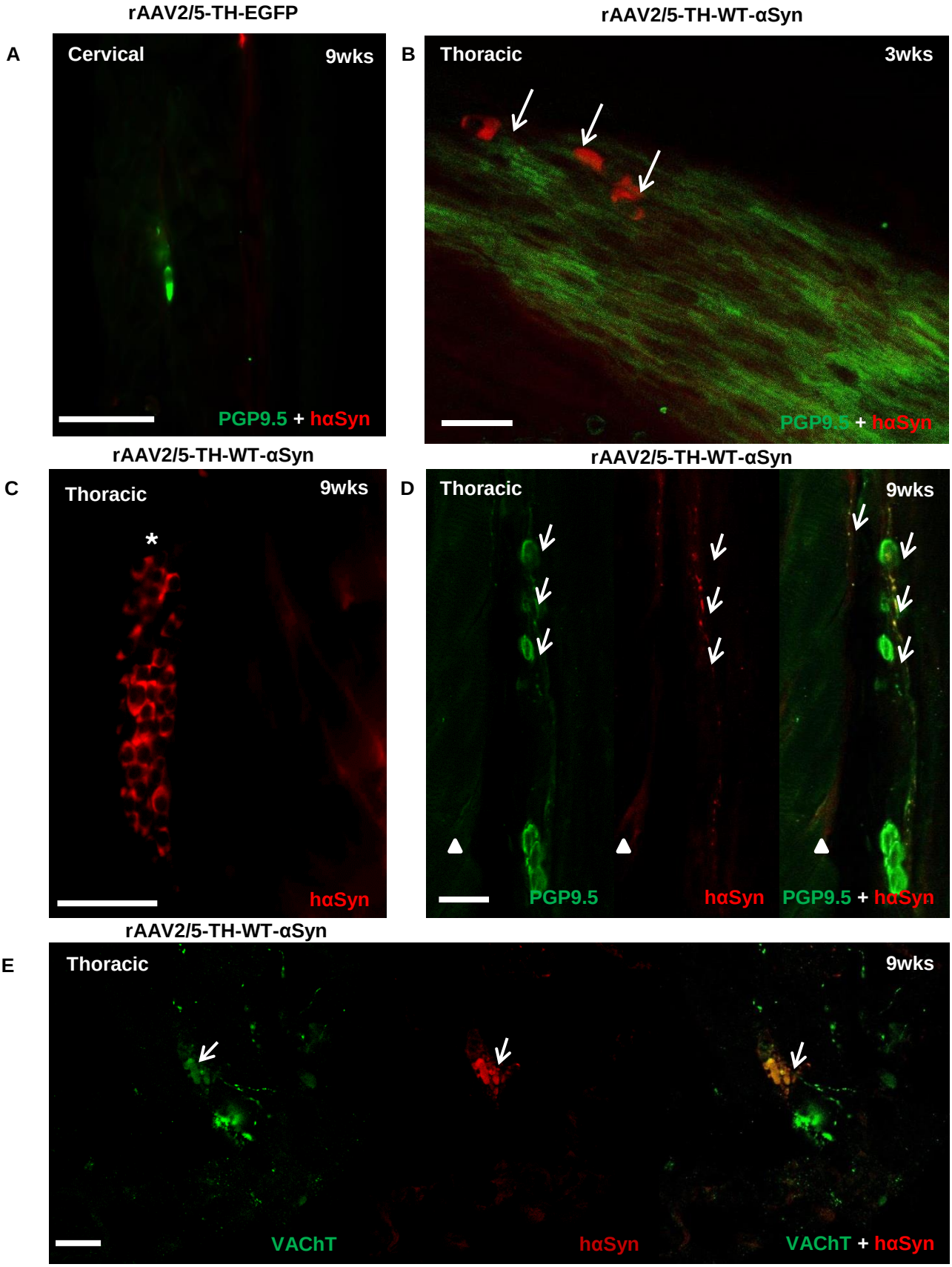
rAAV2/5-TH-EGFP
A
Cervical
9wks
PGP9.5 + hαSyn
rAAV2/5-TH-WT-αSyn
B
Thoracic
3wks
PGP9.5 + hαSyn
rAAV2/5-TH-WT-αSyn
C
Thoracic
9wks
*
hαSyn
rAAV2/5-TH-WT-αSyn
D
Thoracic
9wks
PGP9.5
hαSyn
PGP9.5 + hαSyn
rAAV2/5-TH-WT-αSyn
E
Thoracic
9wks
VAChT
hαSyn
VAChT + hαSyn

Fig. 6 αSyn transport to the cervical and thoracic portions of the mouse esophagus. (A) αSyn-ir negative intramural structure in the cervical portion of the esophagus from the rAAV2/5-TH-EGFP group after 9 weeks of the overexpression. (B, arrows) αSyn-ir enteric neurons marked in (red) were observed in the PGP9.5-ir myenteric plexus layer in the thoracic portion of the esophagus 3 weeks after injection of rAAV2/5-TH-WT-αSyn. (C, asterisk) αSyn-ir myenteric ganglia in (red) were also found in the thoracic portion after 9 weeks. (D, arrows) PGP9.5-ir myenteric neurons were co-localized with αSyn-ir varicosities in the thoracic portion after 3 weeks. The arrowheads also indicate that αSyn-ir muscle areas. (E, arrows) VAChT-ir vagal motor nerve endings were also immunoreactive for αSyn, showing a clear co-localization in the thoracic portion after 9 weeks (Esophagus image of 4 different mice were selected out of 10 mice, either for 3 or 9 weeks). *Scale bars*: 50 μm (A-C), 100 μm (D) and 25 μm (E).

Abnormal VAChT-ir vagal motor efferent projections to the mouse esophagus

To further clarify if the αSyn expression in the motor endings of the striated muscle would disturb the cholinergic vagal efferents in the esophagus or not, co-immunolabeling with VAChT and α-BT was performed in every section of the esophageal tissue. These structures were reported to be always paired as oval shapes over both the inner and outer striated muscle layers [52]. We investigated the cholinergic efferents terminating on the motor endplates of the esophagus either 3 or 9 weeks post the microinjection in the LC. Unlike the majority of the VAChT- and α-BT-ir structures, a certain group of VAChT-ir nerve endings was scattered around but not placed directly on the motor end plates. (Fig.7 A-E). Surprisingly, motor endplates identified with α-BT were found to be adjacent to αSyn-ir structures and immunostaining intensity of the VAChT-ir nerve endings was diminished (Fig. 7 F). In contrast, we did not find the abnormal motor endings in the rAAV2/5-TH-EGFP group (data not shown). This corroborates our hypothesis that αSyn induced dysregulation of the cholinergic efferent projection system in the striated muscles of the esophagus as well, possibly due to the intracellular αSyn in the ambiguus neurons followed by severely suppressed ChAT expression in both hemispheres. Suggestive schematic illustration of the proposed transport circuit via the anatomically connected regions in our model is demonstrated herein (Fig. 8).

rAAV2/5-TH-WT-αSyn

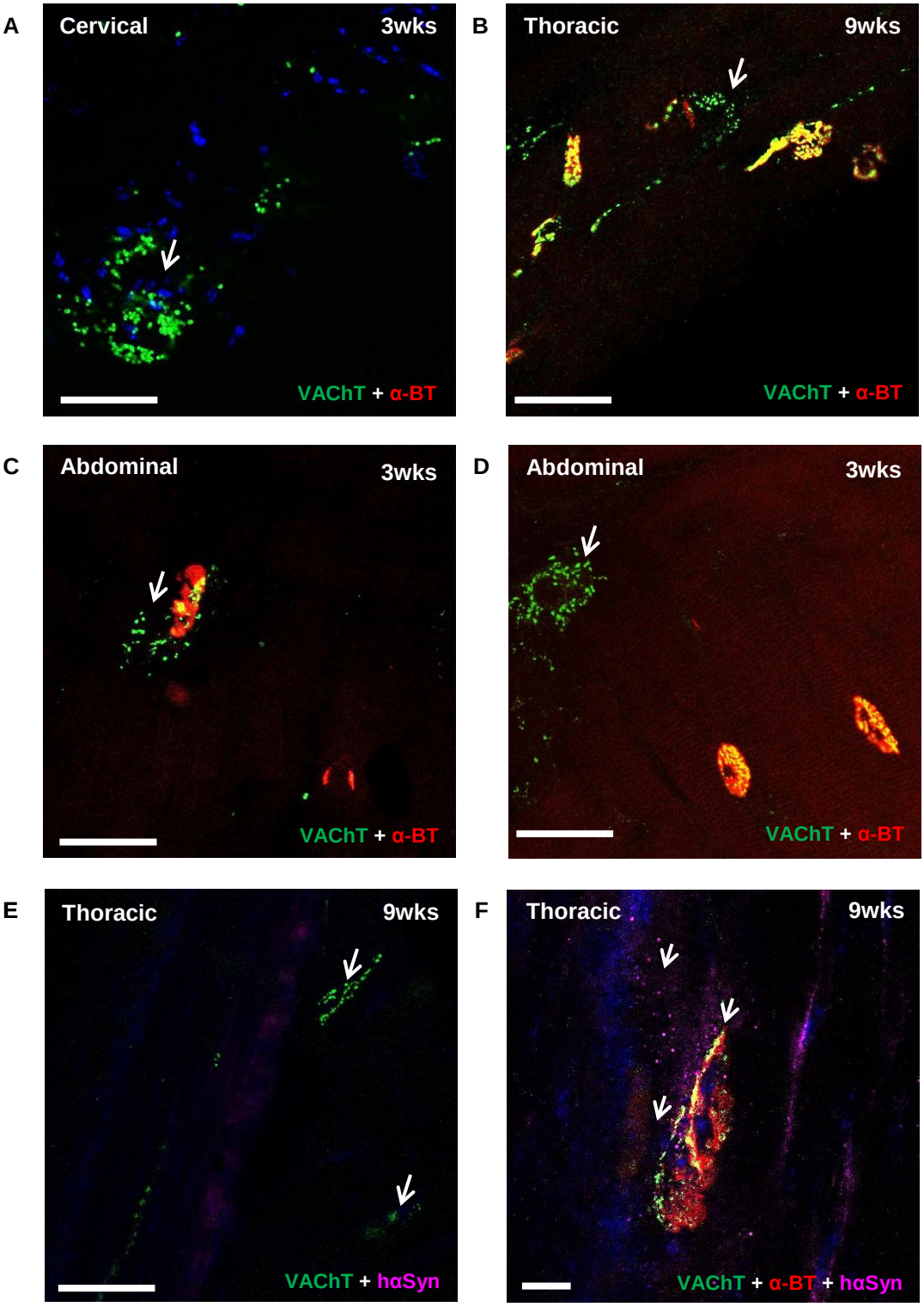

Fig. 7 Abnormal efferent projections from the vagal motor nuclei in the mouse esophagus. (A, arrow) scattered VAChT-ir vagal motor nerve endings marked in (green) were found at the cervical portion of the esophagus without α-BT co-expression labeled in (red). (B-E, arrows) Dispersed and dislocated vagal motor endings around the α-BT-ir motor endplates were found in the thoracic or abdominal portions as early as 3 weeks post the αSyn overexpression in the LC. These abnormal structures were differentiated from the neighboring normal motor endings and the receptors (merged). (E, arrows) Display of the α-BT-ir motor endplates labeled in (red) and vagal motor endings in (green). αSyn-ir cellular structures were labeled in (magenta), and these signals were in close contact in the cervical portion after 9 weeks (Esophagus image of 5 different mice were selected out of 10 mice, either for 3 or 9 weeks). *Scale bar*: 50 μm for (A-E) and 25 μm for (F).

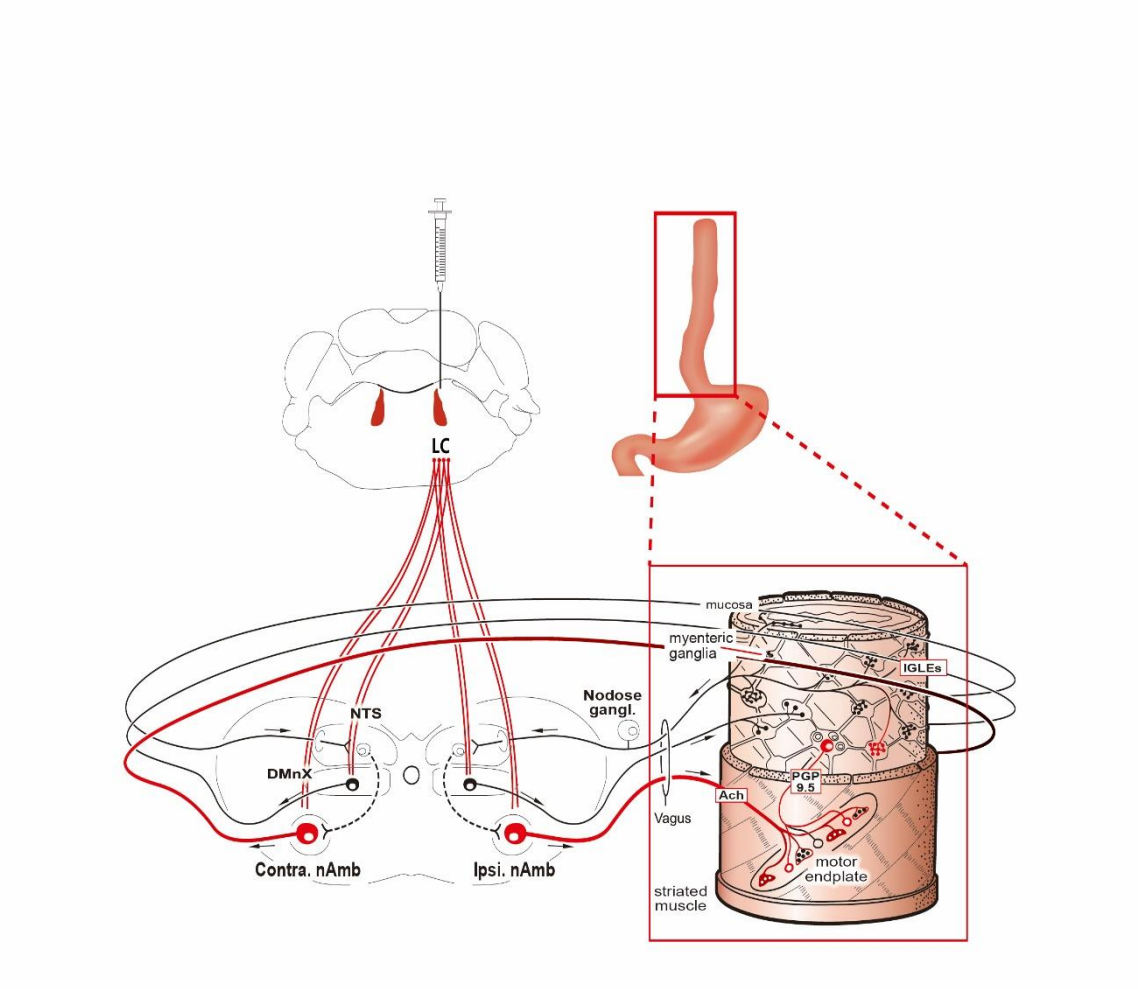

Fig. 8 Schematic illustration demonstrating the noradrenergic modulation of the vago-vagal nuclei and the proposed circuit of αSyn transport to the mouse esophagus. Prof. W.L Neuhuber kindly permitted to re-create the cartoon from his early work, *W.L. Neuhuber et al. 1998*. Unilateral αSyn overexpression in the LC leads to the occurrence of αSyn-ir axonal varicosities in the DMnX and to intraneuronal αSyn in the nAmb in both the contra and ipsilateral sides. Thereafter, these ambiguus neurons transfer the αSyn protein through the vagal efferent system to motor endings of the striated muscle. As these cholinergic axons reaching motor endplates issue collaterals to the myenteric neuronal ganglia of the esophagus (Neuhuber and Wörl, 2016), αSyn may further propagate to the ENS system via these anatomical connections.

ACh: acetylcholine; nAmb: nucleus ambiguus; DMnX: the dorsal motor nucleus of the vagus; IGLEs: intraganglionic laminar endings; NO: nitric oxide; NTS: the nucleus of the solitary tract; VIP: vasoactive intestinal peptide.

Discussion

In the present study, we performed two sets of experiments to understand to what extent noradrenergic LC neurons are vulnerable to WT-αSyn overexpression, and how transduced αSyn in the LC disturbs the vagal motor nuclei, DMnX, and nAmbs, which are known to be vulnerable based on the PD-staging model. In the first part of the study, noradrenergic LC neurons were directly transduced with WT-αSyn via injection of non-specific CMV promoter-dependent viral vectors carrying the genetic information for αSyn. In this model, overexpression of αSyn induced a less than 20% reduction of TH-ir neurons within 9 weeks. Interestingly, prominent micro-astrogliosis was observed already as early as 3 weeks after the onset of WT-αSyn overexpression, presumably due to the release of αSyn from LC neurons in this region [20]. This may demonstrate that micro-and astroglia became reactive due to αSyn derived from the LC neurons, and implies that glial cells may take part in initiating further neuroinflammatory processes before LC cells start to degenerate [27, 28]. In addition, the cholinergic neurons in the DMnX and nAmbs showed a significant decrease of ChAT-ir neuronal numbers as early as 3 weeks, implying a potential toxic effect of αSyn originating from the LC on the vagal motor nuclei. The putative anatomical projection from the noradrenergic LC to the DMnX and to the nAmbs was further confirmed in the second set of experiments using a new TH promoter specific WT-αSyn overexpression model. We clearly show αSyn-ir axonal structures around the DMnX and the nAmb, and this αSyn expression was not limited to the ipsilateral side of the injected LC. Moreover, ambiguus neurons in both the right and the left hemispheres even showed intracellular proteinaceous αSyn along with a significantly reduced ChAT-ir intensity in this model.

A series of literature indicates that the main brainstem circuit that controls swallowing involves the motor nuclei, NTS, DMnX, nAmb and the hypoglossal nucleus which innervate the intrinsic and extrinsic muscles of the tongue, the pharynx, larynx, and esophagus [9, 22, 48]. Especially the early tracing experiments demonstrate well that the origin of extrinsic neurons in the cervical and the abdominal parts of the esophagus is the compact formation of the ambiguus motor neurons [5, 18, 40]. Nevertheless, most experimental effort in the context of αSyn - or toxin-induced PD models has been devoted to the stomach and lower gastrointestinal tracts, less attention has been paid to the esophagus [16, 21, 34]. Therefore, we collected the esophagus

tissues from our mouse models to investigate if robust αSyn-ir varicosities and intracellular αSyn in the ambiguus neurons could also lead to the transport of αSyn to the striated muscles of the esophagus. Notably, we observed αSyn inclusions and fine varicosities in the lamina muscularis mucosae of the cervical, thoracic and abdominal sections of the esophagus. Additional VAChAT and PGP 9.5 co-immunostaining results revealed that αSyn is present in both vagal motor endings and myenteric ganglia as early as 3 weeks post the microinjection in the LC. In contrast, αSyn expression was negative in the rAAV2/5-TH-EGFP group.

Studies show that the nAmb sends collaterals to both motor endplates and enteric ganglia in the esophagus [36], which implies that these motor endplates in the esophagus could represent a "meeting point" of extrinsic vagal cholinergic and intrinsic neurons [56]. Moreover, the enteric co-innervation with vagal motor neurons gates an access to striated muscle to be modulated in parallel because the myenteric neurons are open for both the DMnX and the nucleus ambiguus [18, 32, 33]. This anatomical connection supports our observations that αSyn transport occurred via the closely interconnected brain regions, from the LC to the ambiguus neurons, and again to the vagal motor endings and receptors in the esophagus even within the short time periods. Our results regarding the esophagus are in line with this anatomical connection, and they may functionally imply that αSyn propagated from the LC may disturb not only the cholinergic modulation but also the autonomous system in the upper gastrointestinal tract.

The enteric nervous system has been considered to be the starting gateway of spreading of αSyn-aggregates [8, 13]. The αSyn transport has been demonstrated with various forms in multiple brain regions and showed that cell-to-cell transfer of αSyn is not only possible when using αSyn fibrils but can also be observed in AAV models [37, 49, 51]. It was reported that the αSyn protein transport was more pronounced when neurons were active and healthy without overt damage [50]. Our suggestive early PD model in the LC clearly demonstrates that the WT human αSyn overexpression in the noradrenergic neurons did not lead to a prominent neuronal loss after 9 weeks. In contrast, we postulate that these still vital LC neurons initiated transfer of αSyn to ambiguus neurons, and even to the vagal and enteric neurons of the esophagus only after 3 weeks post the microinjection. The neurobiological link between the

noradrenergic neurons in the LC and the ambiguus neurons was demonstrated in a study using an optogenetic modulation technique [54]. The cardiac vagal neurons in the nAmbs were identified with retrograde fluorescent tracer, which was applied to the cardiac surface of parasympathetic ganglia area in transgenic mice that express channel-rhodopsin-2 (ChR2) in TH neurons. By measuring electrophysiological parameters of the cardiac vagal neurons (CVN) concomitantly when photostimulating LC neurons, the researchers demonstrated that noradrenergic neurons inhibit the CVNs that generate parasympathetic activity to the heart. In addition, another supportive evidence exists for the close relationship between the LC and the nAmbs, especially in terms of dysphasia. The results show that PTEN-induced putative kinase 1(Pink)1 -/- rats display early oropharyngeal swallowing deficits measured by videofluoroscopy and increased αSyn levels in the nAmb and a reduction of noradrenergic neurons in the LC were also observed in the histological investigation [11].

Although we did not perform behavioral experiments with our model, it is tempting to speculate that our model can be representative for prodromal or early PD as LC neurons actively propagate αSyn to the peripheral and enteric nervous system level, where clinical manifestations, such as dysphagia, delayed gastric emptying and reduced gastric motility are known as premotor PD symptoms [1, 2, 47]. Furthermore, neuronal projections from the LC to the DMnX was reported through a classical tracing study in the rat [46], but, in contrast to the nigral projection to the DMnX, it has not been revisited with neurological disease perspective so far. [47, 48, 51]. Therefore, herein we demonstrate for the first time a unique model, in which noradrenergic LC neurons can transfer αSyn to the vagal motor endings and myenteric enteric ganglia in the mouse esophagus via the nAmb. A very recent review states that the LC may act as a ‘way station’ of pathological αSyn transport from the periphery to the rest of the brain [55]. We also reported that overexpression of A53T- αSyn in the LC neurons induced abundant αSyn-ir axons in the LC output regions, indicating rapid anterograde axonal Transport of αSyn [20]. Herein we focused on the αSyn transport via the noradrenergic projection to the vago-vagal nuclei and the cholinergic efferent projection to the esophagus. Our results further suggest that the LC may act not only as a ‘way station’, but also as a ‘roundabout’, which opens an exit back to the ENS providing another negative feedback if the initial α-synucleinopathy started from there based on the

staging theory [8].

Part II-6. Summary

(English)

The locus coeruleus (LC) is a small nucleus among the catecholaminergic cell groups, but it has extensively branched axons, and it innervates broad areas in the brain. According to the widely accepted Parkinson's disease (PD) staging model of Braak, the LC is affected by alpha-synuclein (αSyn) pathology at the second stage, but the possible neurochemical changes induced by axonal αSyn-transport from the LC have never been investigated. Therefore, we overexpressed human wild-type αSyn (WT-αSyn) or the control protein Luciferase (Luc) in the mouse LC via unilateral stereotaxic delivery of recombinant adeno-associated viral vectors (rAAV) and subsequently investigated pathological alterations in a time-dependent manner. Unbiased stereology demonstrated that the number of LC neurons did not significantly decrease upon WT-αSyn overexpression, yet rigorous microgliosis and astrogliosis occurred post 3 weeks post-injection. Intriguingly, the number of choline acetyltransferase (ChAT) immunoreactive (ir) neurons in the dorsal motor nucleus of the vagus (DMnX) and in the nucleus ambiguus (nAmb) significantly decreased in the αSyn group as early as 3 weeks. The putative axonal connectivity between the LC and the cholinergic motor nuclei as well as the loss of ChAT-ir were further elucidated by microinjection of Tyrosine Hydroxylase (TH) promoter-specific viral vectors (rAAV2/5-TH-EGFP or WT-αSyn) in the LC. We found robust αSyn-ir axonal varicosities around the DMnX neurons, and remarkably, intraneuronal αSyn was present in the ambiguus neurons in both hemispheres 3 weeks post-injection. As the compact formation of the nAmb controls the esophagus, we investigated the presence of αSyn in the cervical, thoracic and abdominal parts of the esophagus tissues of injected mice. As a result of aSyn overexpression in the LC, we observed αSyn-ir cells and varicosities in the muscle layers, and notably, some of these αSyn-ir neurons co-localized with myenteric plexus ganglia post 3 and 9 weeks. Furthermore, we found that, unlike the majority of the Vesicular Acetylcholine Transporter (VAChT) signals, some nerve endings were weak in signal and dispersed from the motor receptors. Our data reveal that LC neurons induced the transsynaptic and transneuronal spreading of αSyn in the vagal motor nuclei and suppressed cholinergic efferents terminating on motor endplates in the esophagus. It appears that αSyn can travel through anatomically connected brain regions as proposed in the early staging

model of PD; implying α-synucleinopathy in noradrenergic neurons may potentially disturb the cholinergic modulation of the upper gastrointestinal tract rostral-caudally.

(Deutsch)

Der Locus Coeruleus (LC) ist ein kleiner Nukleus unter den katecholaminergen Zellgruppen, aber er hat stark verzweigte Axone und innerviert dadurch große Bereiche im Gehirn. Nach dem akzeptierten Staging-Modell der Parkinson-Krankheit (PD) von Braak ist der LC ab der zweiten Staging-Phase von Alpha-Synuklein (αSyn)-Pathologie betroffen. Die möglichen neurochemischen Veränderungen durch axonale αSyn-Übertragung aus dem LC wurden allerdings bislang nie untersucht. Daher überexprimierten wir humanes Wildtyp αSyn (WT-αSyn) bzw. das Kontrollprotein Luciferase (Luc) im LC durch einseitige stereotaktische Gabe von rekombinanten Adeno-assoziierten Virus (rAAV) Vektoren und untersuchten anschließend pathologische Veränderungen in Abhängigkeit der Zeit. Eine unvoreingenommene Stereologie zeigte, dass die Anzahl der LC-Neuronen nach WT-αSyn-Überexpression nicht signifikant abnahm, jedoch traten 3 Wochen nach der Injektion ausgeprägte Mikrogliose und Astrogliose auf. Interessanterweise nahm die Anzahl der Cholinacetyltransferase (ChAT)-immunoreaktiven (ir) Neurone im dorsalen motorischen Nucleus des Nervus vagus (DMnX) und im Nucleus ambiguus (nAmb) in der αSyn-Gruppe bereits nach 3 Wochen signifikant ab. Die mutmaßliche axonale Konnektivität zwischen dem LC und den cholinergen motorischen Kernen sowie der Verlust von ChAT-ir wurden durch Mikroinjektion von Tyrosin-Hydroxylase (TH) - Promotor-spezifischen viralen Vektoren (rAAV2/5-TH-EGFP/WT-αSyn) in den LC weiter aufgeklärt. Wir fanden robuste αSyn-ir-axonale Varikositäten um die DMnX-Neurone und erstaunlicherweise auch intraneurales αSyn in Neuronen des nAmb in beiden Hemisphären 3 Wochen nach der Injektion. Da die pars compacta des nAmb die Speiseröhre innerviert, suchten wir nach αSyn in den zervikalen, thorakalen und abdominalen Teilen des Ösophagusgewebes der WT-αSyn-injizierten Mäuse und der Kontroll-Mäuse. Als Ergebnis der aSyn-Überexpression im LC beobachteten wir αSyn-ir-Zellen und Varikositäten in den Muskelschichten. Bemerkenswerterweise waren einige dieser αSyn-ir-Neuronen nach 3 und 9 Wochen mit Plexusganglien des Plexus myentericus kolokalisiert. Darüber hinaus fanden wir, dass im Gegensatz zu den meisten Signalen des vesikulären Acetylcholin-Transporter (VAChT) einige Nervenendigungen schwach und von den motorischen Rezeptoren entfernt waren waren.

Unsere Daten zeigen, dass es zu transsynaptischem und transneuronalem „Spreading“ von αSyn vom LC in die vagalen motorischen Kernen kommt, was zur Suppression von cholinergen Efferenzen an den motorischen Endplatten in der Speiseröhre führt. Es scheint, dass αSyn über anatomisch verbundene Hirnregionen wandern kann, wie bereits im Braak Staging-Modell von PD postuliert, und dass eine α-Synuklein-Pathologie in noradrenergen Neuronen möglicherweise die cholinerge Modulation des rostral-kaudalden oberen Gastrointestinaltrakts stört.

REFERENCES

1. Anselmi L, Toti L, Bove C et al. (2017) A Nigro-Vagal Pathway Controls Gastric Motility and Is Affected in a Rat Model of Parkinsonism. Gastroenterology 153(6): 1581–1593. doi: 10.1053/j.gastro.2017.08.069
2. Anselmi L, Toti L, Bove C et al. (2017) Vagally mediated effects of brain stem dopamine on gastric tone and phasic contractions of the rat. Am J Physiol Gastrointest Liver Physiol 313(5): G434-G441. doi: 10.1152/ajpgi.00180.2017
3. Benarroch EE (2009) The locus ceruleus norepinephrine system. Functional organization and potential clinical significance. Neurology 73(20): 1699–1704. doi: 10.1212/WNL.0b013e3181c2937c
4. Berridge CW, Waterhouse BD (2003) The locus coeruleus-noradrenergic system. Modulation of behavioral state and state-dependent cognitive processes. Brain Res Brain Res Rev 42(1): 33–84
5. Bieger D, Hopkins DA (1987) Viscerotopic representation of the upper alimentary tract in the medulla oblongata in the rat. The nucleus ambiguus. J Comp Neurol 262(4): 546–562. doi: 10.1002/cne.902620408
6. Boeve BF, Silber MH, Saper CB et al. (2007) Pathophysiology of REM sleep behaviour disorder and relevance to neurodegenerative disease. Brain 130(Pt 11): 2770–2788. doi: 10.1093/brain/awm056
7. Braak H, Del Tredici K (2017) Neuropathological Staging of Brain Pathology in Sporadic Parkinson's disease. Separating the Wheat from the Chaff. J Parkinsons Dis 7(s1): S73-S87. doi: 10.3233/JPD-179001
8. Braak H, Del Tredici K, Rüb U et al. (2003) Staging of brain pathology related to sporadic Parkinson's disease. Neurobiol Aging 24(2): 197–211
9. Broussard DL, Altschuler SM (2000) Brainstem viscerotopic organization of afferents and efferents involved in the control of swallowing. Am J Med 108 Suppl 4a: 79S-86S
10. Chiu W-H, Carlsson T, Depboylu C et al. (2014) Selegiline normalizes, while l-DOPA sustains the increased number of dopamine neurons in the olfactory bulb in a 6-OHDA mouse model of Parkinson's disease. Neuropharmacology 79: 212–221. doi: 10.1016/j.neuropharm.2013.11.014
11. Cullen KP, Grant LM, Kelm-Nelson CA et al. (2018) Pink1 -/- Rats Show Early-Onset Swallowing Deficits and Correlative Brainstem Pathology. Dysphagia. doi: 10.1007/s00455-018-9896-5
12. Del Tredici K, Braak H (2013) Dysfunction of the locus coeruleus-norepinephrine system and related circuitry in Parkinson's disease-related dementia. J Neurol Neurosurg Psychiatry 84(7): 774–783. doi: 10.1136/jnnp-2011-301817
13. Del Tredici K, Braak H (2016) Review. Sporadic Parkinson's disease: development and distribution of α-synuclein pathology. Neuropathol Appl Neurobiol 42(1): 33–50. doi: 10.1111/nan.12298

14. Feinstein DL, Kalinin S, Braun D (2016) Causes, consequences, and cures for neuroinflammation mediated via the locus coeruleus. Noradrenergic signaling system. J Neurochem 139 Suppl 2: 154–178. doi: 10.1111/jnc.13447
15. Ganjam GK, Benzler J, Pinkenburg O et al. (2013) Overexpression of suppressor of cytokine signaling 3 in the arcuate nucleus of juvenile Phodopus sungorus alters seasonal body weight changes. J Comp Physiol B, Biochem Syst Environ Physiol 183(8): 1101–1111. doi: 10.1007/s00360-013-0772-1
16. Giancola F, Torresan F, Repossi R et al. (2017) Downregulation of neuronal vasoactive intestinal polypeptide in Parkinson's disease and chronic constipation. Neurogastroenterol Motil 29(5). doi: 10.1111/nmo.12995
17. Hawkes CH, Del Tredici K, Braak H (2007) Parkinson's disease. A dual-hit hypothesis. Neuropathol Appl Neurobiol 33(6): 599–614. doi: 10.1111/j.1365-2990.2007.00874.x
18. Hayakawa T, Kuwahara S, Maeda S et al. (2008) Direct synaptic projections to the myenteric ganglion of the rat subdiaphragmatic esophagus from the dorsal motor nucleus of the vagus. Neurosci Res 61(4): 368–374. doi: 10.1016/j.neures.2008.04.004
19. Heneka MT, Nadrigny F, Regen T et al. (2010) Locus ceruleus controls Alzheimer's disease pathology by modulating microglial functions through norepinephrine. Proc Natl Acad Sci U S A 107(13): 6058–6063. doi: 10.1073/pnas.0909586107
20. Henrich MT, Geibl FF, Lee B et al. (2018) A53T-α-synuclein overexpression in murine locus coeruleus induces Parkinson's disease-like pathology in neurons and glia. Acta Neuropathol Commun 6(1): 39. doi: 10.1186/s40478-018-0541-1
21. Holmqvist S, Chutna O, Bousset L et al. (2014) Direct evidence of Parkinson pathology spread from the gastrointestinal tract to the brain in rats. Acta Neuropathol 128(6): 805–820. doi: 10.1007/s00401-014-1343-6
22. Jean A (2001) Brain stem control of swallowing. Neuronal network and cellular mechanisms. Physiol Rev 81(2): 929–969. doi: 10.1152/physrev.2001.81.2.929
23. Kalia M (1981) Brain stem localization of vagal preganglionic neurons. J Auton Nerv Syst 3(2-4): 451–481
24. Kelly SC, He B, Perez SE et al. (2017) Locus coeruleus cellular and molecular pathology during the progression of Alzheimer’s disease. Acta Neuropathol Commun 5. doi: 10.1186/s40478-017-0411-2
25. Koprich JB, Kalia LV, Brotchie JM (2017) Animal models of α-synucleinopathy for Parkinson disease drug development. Nat Rev Neurosci 18(9): 515–529. doi: 10.1038/nrn.2017.75
26. Lang AE (2011) A critical appraisal of the premotor symptoms of Parkinson's disease. Potential usefulness in early diagnosis and design of neuroprotective trials. Mov Disord 26(5): 775–783. doi: 10.1002/mds.23609
27. Lee H-J, Suk J-E, Patrick C et al. (2010) Direct transfer of alpha-synuclein from neuron to astroglia causes inflammatory responses in synucleinopathies. J Biol Chem 285(12): 9262–9272. doi: 10.1074/jbc.M109.081125

28. Lim S, Chun Y, Lee JS et al. (2016) Neuroinflammation in Synucleinopathies. Brain Pathol 26(3): 404–409. doi: 10.1111/bpa.12371
29. Luk KC, Kehm V, Carroll J et al. (2012) Pathological α-synuclein Transport initiates Parkinson-like neurodegeneration in nontransgenic mice. Science 338(6109): 949–953. doi: 10.1126/science.1227157
30. Marien M, Briley M, Colpaert F (1993) Noradrenaline depletion exacerbates MPTP-induced striatal dopamine loss in mice. Eur J Pharmacol 236(3): 487–489
31. Meles SK, Renken RJ, Janzen A et al. (2018) The metabolic pattern of idiopathic REM sleep behavior disorder reflects early-stage Parkinson's disease. J Nucl Med. doi: 10.2967/jnumed.117.202242
32. Neuhuber WL, Kressel M, Stark A et al. (1998) Vagal efferent and afferent innervation of the rat esophagus as demonstrated by anterograde DiI and DiA tracing. Focus on myenteric ganglia. J Auton Nerv Syst 70(1-2): 92–102
33. Neuhuber WL, Wörl J (2016) Enteric co-innervation of striated muscle in the esophagus. Still enigmatic? Histochem Cell Biol 146(6): 721–735. doi: 10.1007/s00418-016-1500-1
34. Noorian AR, Rha J, Annerino DM et al. (2012) Alpha-synuclein transgenic mice display age-related slowing of gastrointestinal motility associated with transgene expression in the vagal system. Neurobiol Dis 48(1): 9–19. doi: 10.1016/j.nbd.2012.06.005
35. Paxinos G, Franklin KBJ (2013) Paxinos and Franklin's the mouse brain in stereotaxic coordinates, Fourth edition. Elsevier Academic Press, Amsterdam, Boston, Heidelberg
36. Powley TL, Mittal RK, Baronowsky EA et al. (2013) Architecture of Vagal Motor Units Controlling Striated Muscle of Esophagus. Peripheral Elements Patterning Peristalsis? Auton Neurosci 179(0). doi: 10.1016/j.autneu.2013.08.069
37. Recasens A, Ulusoy A, Kahle PJ et al. (2017) In vivo models of alpha-synuclein Transport and propagation. Cell Tissue Res. doi: 10.1007/s00441-017-2730-9
38. Rey NL, Steiner JA, Maroof N et al. (2016) Widespread transneuronal propagation of alpha-synucleinopathy triggered in olfactory bulb mimics prodromal Parkinson's disease. J Exp Med 213(9): 1759–1778. doi: 10.1084/jem.20160368
39. Rommelfanger KS, Weinshenker D (2007) Norepinephrine. The redheaded stepchild of Parkinson's disease. Biochem Pharmacol 74(2): 177–190. doi: 10.1016/j.bcp.2007.01.036
40. Sang Q, Young HM (1998) The origin and development of the vagal and spinal innervation of the external muscle of the mouse esophagus. Brain Res 809(2): 253–268
41. Schindelin J, Arganda-Carreras I, Frise E et al. (2012) Fiji. An open-source platform for biological-image analysis. Nat Methods 9(7): 676–682. doi: 10.1038/nmeth.2019
42. Schwarz LA, Luo L (2015) Organization of the locus coeruleus-norepinephrine system. Curr Biol 25(21): R1051-R1056. doi: 10.1016/j.cub.2015.09.039

43. Sommerauer M, Fedorova TD, Hansen AK et al. (2017) Evaluation of the noradrenergic system in Parkinson's disease. An 11C-MeNER PET and neuromelanin MRI study. Brain. doi: 10.1093/brain/awx348
44. Surmeier DJ, Sulzer D (2013) The pathology roadmap in Parkinson disease. Prion 7(1): 85–91. doi: 10.4161/pri.23582
45. Szabadi E (2013) Functional neuroanatomy of the central noradrenergic system. J Psychopharmacol (Oxford) 27(8): 659–693. doi: 10.1177/0269881113490326
46. Ter Horst GJ, Toes GJ, van Willigen JD (1991) Locus coeruleus projections to the dorsal motor vagus nucleus in the rat. Neuroscience 45(1): 153–160
47. Toti L, Travagli RA (2014) Gastric dysregulation induced by microinjection of 6-OHDA in the substantia nigra pars compacta of rats is determined by alterations in the brain-gut axis. Am J Physiol Gastrointest Liver Physiol 307(10): G1013-23. doi: 10.1152/ajpgi.00258.2014
48. Travagli RA, Anselmi L (2016) Vagal neurocircuitry and its influence on gastric motility. Nat Rev Gastroenterol Hepatol 13(7): 389–401. doi: 10.1038/nrgastro.2016.76
49. Ulusoy A, Rusconi R, Pérez-Revuelta BI et al. (2013) Caudo-rostral brain spreading of α-synuclein through vagal connections. EMBO Mol Med 5(7): 1119–1127. doi: 10.1002/emmm.201302475
50. Ulusoy A, Musgrove RE, Rusconi R et al. (2015) Neuron-to-neuron α-synuclein propagation in vivo is independent of neuronal injury. Acta Neuropathol Commun 3. doi: 10.1186/s40478-015-0198-y
51. Ulusoy A, Phillips RJ, Helwig M et al. (2017) Brain-to-stomach transfer of α-synuclein via vagal preganglionic projections. Acta Neuropathol 133(3): 381–393. doi: 10.1007/s00401-016-1661-y
52. van der Keylen P, Garreis F, Steigleder R et al. (2016) Involvement of catecholaminergic neurons in motor innervation of striated muscle in the mouse esophagus. Histochem Cell Biol 145(5): 573–585. doi: 10.1007/s00418-015-1403-6
53. Vermeiren Y, Deyn PP de (2017) Targeting the norepinephrinergic system in Parkinson's disease and related disorders. The locus coeruleus story. Neurochem Int 102: 22–32. doi: 10.1016/j.neuint.2016.11.009
54. Wang X, Piñol RA, Byrne P et al. (2014) Optogenetic Stimulation of Locus Ceruleus Neurons Augments Inhibitory Transport to Parasympathetic Cardiac Vagal Neurons via Activation of Brainstem α1 and β1 Receptors. J Neurosci 34(18): 6182–6189. doi: 10.1523/JNEUROSCI.5093-13.2014
55. Weinshenker D (2018) Long Road to Ruin. Noradrenergic Dysfunction in Neurodegenerative Disease. Trends Neurosci 41(4): 211–223. doi: 10.1016/j.tins.2018.01.010
56. Wörl J, Neuhuber WL (2005) Enteric co-innervation of motor endplates in the esophagus. State of the art ten years after. Histochem Cell Biol 123(2): 117–130. doi: 10.1007/s00418-005-0764-7

Acknowledgment

First of all, I sincerely thank Sabine Anfimov and Christine Höft for all their technical support for the experiments done in Marburg. I also thank Karin Löschner and Stephanie Link for histology work in Erlangen. I would like to acknowledge the Core Facility Cellular Imaging of the Philipps University-Marburg for the use of the Leica confocal microscope and Zeiss spinning disc microscope. We deeply thank Katrin Roth for the technical supervision for the high-quality micrographs.

Last but not least, I deeply appreciate my family and friends who supported me during my studying in Marburg. In addition, Prof. Wolfgang Oertel helped me a lot from the beginning until now. I sincerely thank him for providing me with a wonderful opportunity to work in neuroscience research again. His supervision strongly motivated me to come this far with my own thesis, and I feel very blessed.